1   **Functional memory T cells are derived from exhausted clones and expanded by checkpoint**
2   **blockade**
3
4   Colin J. Raposo[1,2], Patrick K. Yan[1,2], Andy Y. Chen[1,3], Saba Majidi[1], Kamir J. Hiam-Galvez[1,*], and
5   Ansuman T. Satpathy[1,4,5,*]
6
7   [1] Department of Pathology, Stanford University, Stanford, CA, USA
8   [2] Program in Immunology, Stanford University, Stanford, CA, USA
9   [3] Department of Bioengineering, Stanford University, Stanford, CA, USA
10   [4] Parker Institute for Cancer Immunotherapy, San Francisco, CA, USA
11   [5] Stanford Cancer Institute, Stanford University, Stanford, CA, USA
12   *Correspondence to: khiamg@stanford.edu and satpathy@stanford.edu
13

Summary

15   Immune checkpoint blockade can facilitate tumor clearance by T cells, resulting in long term patient
16   survival. However, the capacity of exhausted CD8^{+} T cells (Tex), present during chronic antigen
17   exposure, to form memory after antigen clearance remains unclear. Here, we performed longitudinal
18   single cell RNA/T cell receptor sequencing and ATAC-sequencing on antigen-specific T cells after the
19   clearance of chronic lymphocytic choriomeningitis virus (LCMV) infection. These data revealed the
20   formation of a robust population of memory CD8^{+} T cells that transcriptionally, epigenetically, and
21   functionally resemble central memory T cells (Tcm) that form after clearance of acute infection. To lineage
22   trace the origin and memory recall response of Tex-derived memory clones, we utilized T cell receptor
23   sequencing over the course of primary infection and rechallenge. We show that chronic Tcm are a clonally
24   distinct lineage of Tex derived from progenitor exhausted cells, persist long-term in the absence of
25   antigen, and undergo rapid clonal expansion during rechallenge. Finally, we demonstrate that αPD-L1
26   immune checkpoint blockade after chronic LCMV infection preferentially expands clones which form Tcm
27   after clearance. Together, these data support the concept that chronically stimulated T cells form *bona*
28   *fide* functional memory T cells through an analogous differentiation pathway to acutely stimulated T cells,
29   which may have significant implications for enhancing immune memory to cancer through checkpoint
30   blockade and vaccination.

Main

31

32   Persistent antigen present during cancer and chronic infection drives CD8^{+} T cell exhaustion – a cell
33   state categorized by the expression of co-inhibitory receptors (e.g. PD-1, Tim-3, Lag-3) and decreased
34   cytokine production, proliferation, and target cell killing[1–8]. Recent developments in high-throughput
35   genomic technologies, including single cell RNA, T cell receptor (TCR), and assay for transposase-
36   accessible chromatin (ATAC) sequencing have provided new insights into the functional subsets,
37   molecular regulation, and clonal differentiation pathways of exhausted T cells (Tex). These studies have
38   revealed that Tex are a functionally diverse cellular pool that includes hypofunctional terminally
39   exhausted cells (Tex-Term), effector-like intermediate cells (Tex-Int), killer cell lectin-like receptor-
40   expressing exhausted cells (Tex-KLR), and stem-like progenitor exhausted cells (Tex-Prog) that reseed
41   other Tex populations and respond to immune checkpoint blockade (ICB; ref[9–16]). The ability to track
42   individual T cell clones using TCR sequencing has provided even greater resolution of Tex differentiation
43   and revealed that individual Tex clones can exhibit a bias towards either Tex-Term or Tex-KLR terminally
44   differentiated states[11]. Finally, epigenetic profiling has demonstrated that Tex represent a distinct
45   differentiation trajectory that is accompanied by genome-wide changes in chromatin accessibility that
46   limit subsequent activation following antigen recognition[17,18].

47   Despite these advances in understanding of Tex differentiation, the field lacks a similar level of insight
48   into the long-term impact of chronic stimulation on the generation of T cell memory. After the clearance
49   of antigen from acute infections or vaccination, the antigen-specific T cell compartment contracts, and
50   the remaining cells form long-lived memory T cells[19,20]. Upon reexposure to antigen, memory T cells
51   expand and differentiate more rapidly than naive T cells and provide protection against reinfection[21,22].
52   However, after the clearance of chronic antigens, antigen-specific T cells persist long-term, but are not
53   thought to provide the enhanced protection after reinfection characteristic of memory T cells[23,24]. While
54   persisting T cells can express some markers of T cell memory (e.g. CD127, CD62L, TCF-1) after chronic
55   antigen clearance, their ability to re-expand is lower than acute memory T cells, and this functional
56   difference has been explained by epigenetic differences resulting from chronic stimulation[4,23,25–28].
57   Namely, chronic memory-like cells have increased accessibility of loci which encode for exhaustion
58   related transcription factors (e.g. *Tox, Tox2,* and *Batf*) and co-inhibitory receptors (e.g. *Pdcd1*, *Lag3*, and
59   *Tigit*) and decreased accessibility of effector function-associated gene loci[25,28]. These changes reinforce
60   a Tex cell state upon stimulation and lead to decreased expansion, effector cell differentiation, and
61   production of proinflammatory cytokines, including interferon (IFN)-γ and tumor necrosis factor (TNF)-
62   α[26–28]. However, to date, these functional and epigenetic studies have largely been performed on
63   aggregate Tex populations, typically for a single TCR specificity, rather than on individual clones within
64   a polyclonal T cell response. Thus, it is unclear whether all antigen-specific clones maintain a
65   dysfunctional phenotype following clearance of chronic antigen or whether a subset of Tex clones may
66   be able to generate functional memory T cells.

67   Here, we leveraged high-throughput single cell RNA and TCR sequencing (scRNA/TCR-seq) to
68   understand the cellular and clonal heterogeneity of antigen-specific T cells after the clearance of chronic
69   viral infection. We show that antigen-specific T cells form a population of central memory T cells (Tcm)
70   that have a shared transcriptional and epigenomic profile with Tcm formed after the clearance of acute
71   infection. Through longitudinal profiling of the TCR repertoire, we show that chronic Tcm (cTcm) derive
72   from a distinct differentiation trajectory of Tex-Prog biased clones present during chronic infection, and
73   upon rechallenge exhibit enhanced capacity to expand and differentiate, promoting viral clearance.
74   Finally, utilizing longitudinal TCR repertoire analysis over the course of infection, we demonstrate that
75   ICB preferentially expands and differentiates clones that form cTcm while preserving their memory
76   function. Altogether, these findings demonstrate the capacity of a clonally-restricted subset of Tex clones

77 to form highly functional memory cells and highlight the potential of therapeutic interventions to enhance
78 memory responses to chronic infections or cancer.
79

Antigen-specific memory T cells are formed after the clearance of chronic viral infection

81   To study the clonal differentiation patterns of antigen-specific T cells after the clearance of chronic
82 antigen exposure, we performed scRNA/TCR-seq on antigen-specific T cells from the spleen after the
83 peripheral clearance of chronic lymphocytic choriomeningitis virus clone-13 (LCMV-Cl13), achieved by
84 100 days post infection (dpi; **Extended Data Fig. 1a**; ref[1]). We analyzed transcriptomes of GP33:H2-D^b
85 tetramer-reactive T cells (GP33$^+$), GP33$^+$ CD62L$^+$ T cells (to enrich for memory-like cells), or GP33$^+$
86 CD62L$^-$ CD8$^+$ T cells: (1) after peripheral clearance of LCMV-Cl13 (100+ dpi), (2) during LCMV-Cl13
87 infection (21-26 dpi), or (3) after clearance of the acute LCMV-Armstrong (LCMV-Arm; 60+ dpi; **Fig. 1a,b,**
88 **Extended Data Fig. b-d**). Clustering of cells (n=34,269) identified distinct exhausted and memory T cell
89 subsets based on differential gene expression (LogFC>0.25; **Fig. 1b,c**; **Supplementary Table 1**). During
90 chronic infection, GP33$^+$ T cells comprised Tex clusters, including Tex-Term, characterized by high
91 expression of *Pdcd1* (encoding PD-1), *Tox,* and *Cd101* (**Fig. 1c,d**). Effector gene expression (*Cx3cr1,*
92 *Zeb2, and Klrg1*) along with *Pdcd1* and *Tox* expression identified Tex-Int and Tex-KLR (**Fig. 1c,d**). Tex-
93 Prog were identified by high expression of *Slamf6* (encoding Ly108), *Tcf7* (encoding T Cell Factor [TCF]-
94 1), *Pdcd1*, and *Tox* (**Fig. 1c,d**). After LCMV-Arm clearance, GP33$^+$ cells comprised canonical memory
95 cell clusters, including Tcm (expressing *Sell* [encoding CD62L]*, Tcf7,* and *Il7r* [encoding CD127]) and
96 effector memory cell (Tem; expressing *Il7r, Cx3cr1,* and *Zeb2*) states (**Fig. 1c,d**). Unexpectedly, while
97 canonical Tex subsets found in earlier time points persisted post peripheral LCMV-Cl13 clearance, the
98 majority of GP33$^+$ cells clustered with either acute Tem or Tcm, suggesting that Tex can differentiate to
99 form cells with transcriptional phenotypes that are highly similar to Tcm and Tem (**Fig. 1d**).
100   To better understand the transcriptional state of chronic memory cells, we compared cTcm and
101 chronic Tem (cTem; defined by similarity to Tem in acute infection) to other subsets based on scRNA-
102 seq profiles. Global comparisons by principal component analysis (PCA) showed significantly correlated
103 gene expression between Tcm derived from both infection contexts (*P*<0.001; **Fig. 1e**). Likewise, gene
104 expression profiles of cTem from both infection contexts were also significantly correlated (*P*<0.001; **Fig.**
105 **1e**). Next, we performed differential expression analysis between cTcm and acute Tcm (aTcm), as well
106 as cTem and acute Tem (aTem; **Fig. 1f**). Overall, there were fewer differentially expressed genes (DEGs;
107 *P*<0.01, Log$_2$FC>0.25; **Supplementary Table 2**) between cTcm and aTcm (n=56) than between cTcm
108 and every other Tex subset from chronic infection (n≥391; **Fig 1f**). Similarly, there were fewer DEGs
109 between cTem and aTem (n=95) than between cTem and other Tex subsets (n≥226; **Fig 1f**). The few
110 DEGs that were more highly expressed in chronic memory cells were consistent with Tex origin, including
111 *Tox*, *Pdcd1*, and the interferon stimulated gene *Ifi27l2a*, which were higher in cTcm/cTem versus
112 aTcm/aTem (**Supplementary Table 2**). Conversely, aTcm and aTem had increased expression of
113 activator protein-1 (AP-1) family transcription factors (*Jun, Junb, Jund*) and the chromatin remodeler
114 *Satb1*, compared to cTcm and cTem, consistent with increased AP-1 activity in effector cells compared
115 to Tex (**Supplementary Table 2**; ref[29]). Finally, we compared expression of a module of core exhaustion
116 genes (including *Tox, Pdcd1, Tigit,* and *Lag3*; **Supplementary Table 7**; ref[11]) between cells subsets post-
117 LCMV-Cl13 clearance, which showed that cTcm cells had a lower exhaustion module score (-0.077) than
118 Tex clusters (Tex-Term=0.84, Tex-Prog=0.081, Tex-Int=0.39, Tex-KLR=0.076), and the exhaustion
119 module score of cTcm was similar to that of aTcm (-0.12; **Extended Data Fig. 1e**).
120   To validate the presence of chronic cTcm using an orthogonal assay, we performed flow cytometry
121 on GP33$^+$ T cells from the same time points as scRNA/TCR-seq. Consistent with the scRNA/TCR-seq
122 data, GP33$^+$ T cells had significantly decreased PD-1$^+$ cell frequency (FC=3.34 *P*=0.0095) and increased
123 CD127$^+$ cell frequency (FC=8.58 *P*=0.0095) at 100+ dpi compared to 21 dpi (**Extended Data Fig. 2a**).

124 Similarly, we observed a significant increase in the frequency of CD127^{+} CD62L^{+} T cells (canonical Tcm
125 markers) from 21 to 100+ dpi (FC=4.01 *P*=0.0095; **Extended Data Fig. 2a**). CD127^{+} CD62L^{+} T cells
126 comprised 6.57% of GP33^{+} T cells (**Extended Data Fig. 2a**). We assessed the frequency of CD127^{+}
127 CD62L^{+} T cells at later time points post- peripheral LCMV clearance and observed that they persisted for
128 at least 350 dpi, suggesting long-term durability of cTcm, similar to Tcm formed after acute infection
129 (**Extended Data Fig. 2b**; ref[30]).

130 To further evaluate functional differences and validate DEGs of chronic memory cells, we developed
131 a flow cytometry gating scheme to identify and compare GP33^{+} cTcm, cTem, Tex-Prog, and Tex-Term
132 at 100+ dpi to aTcm from LCMV-Arm (GP33^{+} CD62L^{+} CXCR3^{+}) and Tex-Prog from ongoing LCMV-Cl13
133 infection (GP33^{+} CX3CR1^{-} Ly108^{+}; **Fig. 1g**). Consistent with scRNA/TCR-seq, GP33^{+} cells were
134 predominantly cTem at 100+ dpi (68.45%), with cTcm (4.23%), Tex-Prog (6.31%), and Tex-Term (2.78%)
135 present at lower relative frequencies (**Fig. 1h**). TCF-1 expression was significantly higher in cTcm than
136 other subsets from cleared LCMV-Cl13 (Tex-Prog: FC=1.13 *P*=0.026, Tex-Term: FC=1.9 *P*=0.0022, Tem
137 1: FC=3.71 *P*=0.0022, Tem 2: FC=3.25 *P*=0.0022; **Fig. 1i,j**). cTcm had significantly lower TOX (FC=2.37
138 *P*=0.0095) and PD-1 (FC=8.38 *P*=0.0095) expression relative to Tex-Prog from 21 dpi. Consistent with
139 scRNA/TCR-seq data, cTcm had elevated PD-1 expression (*P*=0.043) compared to aTcm but decreased
140 expression compared to Tex subsets (Tex-Prog: FC=2.14 *P*=0.013, Tex-Term: FC=4.9 *P*=0.0022, Tex-
141 Prog 21 dpi: FC=8.38 *P*=0.0095; **Fig. 1i,j**). Finally, we evaluated the function of GP33^{+} cell subsets *in*
142 *vitro* by measuring cytokine secretion following stimulation with PMA/Ionomycin. cTcm secreted similar
143 amounts of IFNγ and TNFα as aTcm (*P*>0.05) and significantly higher levels of IFNγ, Interleukin (IL)-2,
144 and TNFα compared to cTem or Tex-Prog from ongoing LCMV-Cl13 infection (*P*<0.05; **Fig. 1k**).
145 Altogether, these data suggest that cTcm formed after the clearance of chronic LCMV infection are
146 transcriptionally, phenotypically, and functionally similar to aTcm.

147

148 **cTcm are derived from Tex-Prog biased clones**
149 Memory and exhausted T cells achieve population-level functional diversity through the differentiation
150 of individual clones with distinct fate distributions[11,31–33]. To assess behaviors of individual T cell clones
151 after peripheral LCMV-Cl13 clearance, we analyzed the scRNA/TCR-seq data and identified 246
152 expanded *Tcra/Tcrb* clones in scRNA/TCR-seq (n>1 cell per clone, average 35 clones per mouse). To
153 identify shared clonal differentiation patterns, we clustered clones based on intraclonal phenotype
154 proportions (**Fig. 2a, Extended Data Fig. 3a**). This analysis revealed five distinct clonal differentiation
155 patterns of GP33^{+} T cells after chronic antigen clearance: cTcm biased clones (n=66), Tem 1 biased
156 clones (n=49), Tem 2 biased clones (n=75), Tex biased clones (n=7), and divergent clones with no
157 preferential fate bias (n=49; **Fig. 2a, Extended Data Fig. 3a**). We next performed bulk TCR β-chain
158 sequencing (TCR-seq) on sorted GP33^{+} T cell subsets (cTcm, Tem 1, Tem 2, Tex-Prog, Tex-Term;
159 **Extended Data Fig. 3b**) for greater TCR sequencing depth and clonal resolution (**Fig. 2b-d**). In this
160 dataset, we identified 190 expanded clones (n>4 cells per clone, average 63 clones per mouse; **Fig. 2b**).
161 Clustering of expanded clones from bulk TCR-seq further confirmed the presence of cTcm biased (n=25),
162 Tem 1 biased (n=41), Tem 2 biased (n=39), and divergent clones (n=48; **Fig. 2b**). In addition, the depth
163 of this dataset also enabled the identification of Tex-Prog biased (n=9) and Tex-Term biased (n=28)
164 biased clones, which were not observed in scRNA/TCR-seq due to low sampling of small clones (**Fig.
165 2b**). Across both scRNA/TCR-seq and bulk TCR-seq data, the majority of cells in cTcm biased clones
166 were cTcm (median=86.6% cTcm in scRNA/TCR-seq, median=66.5% in bulk TCR-seq; **Fig. 2b**,
167 **Extended Data Fig. 3a**). To quantitatively assess intraclonal phenotype distributions, we asked whether
168 clones in each cluster were enriched for a dominant phenotype compared to a background distribution
169 (**Fig. 2c**). Indeed, we found that the majority of clones in Tex-Prog, cTcm, Tex-Term, and Tem 2 biased
170 clusters were significantly enriched for their respective cell subsets (*P*<0.05 hypergeometric test), while

4

171 only 10.4% of divergent clones showed significant enrichment (**Fig. 2c**). Finally, the cTcm subset had
172 low clonal overlap with other T cell subsets, as measured by Morisita-Horn index (Median=0.66; **Fig. 2d**).
173 In contrast, there was high clonal overlap between Tex-Prog / Tex-Term (0.91) and cTem 1 / cTem 2
174 subsets (0.94; **Fig. 2d**). These results demonstrate that cTcm represent a distinct clonal Tex
175 differentiation trajectory and suggest the presence of clonally restricted cTcm precursors during chronic
176 infection.

177   To confirm that the cTcm biased clones were derived from Tex, rather than newly primed after the
178 chronic phase of infection, we compared the TCR repertoire of GP33$^+$ CD8$^+$ T cells from peripheral blood
179 28 dpi to the TCR repertoire in the spleen from the same mice 100+ dpi (**Extended Data Fig. 3c,d**). We
180 detected 25 cTcm biased clones at 100+ dpi, 14 of which were detected in the blood at 28 dpi (56%, 95%
181 confidence interval [CI] = +/-19.5% by logistic regression), confirming that cTcm can indeed emerge from
182 the exhausted T cell pool (**Extended Data Fig. 3d**). To determine whether a specific Tex subset
183 preferentially forms cTcm, we transferred antigen-specific P14 Tex-Prog, Tex-Int, Tex-KLR, and Tex-
184 Term from 21 dpi of LCMV-Cl13 infection into infection-free mice (**Fig. 2e**, **Extended Data Fig. 4e-g**). 22
185 days post transfer, we isolated the progeny of transferred cells and found that cTcm were derived
186 exclusively from Tex-Prog (median=30.9% of Tex-Prog derived cells vs. 0% for other subsets; *P*=0.0079;
187 **Fig. 2e**, **Extended Data Fig. 4f,g**)

188   Since not all transferred Tex-Prog formed CD62L$^+$ cTcm, we asked whether a subset of clones that
189 generate Tex-Prog may preferentially form cTcm after viral clearance. In murine cytomegalovirus
190 infection, T cell clones that express memory associated genes early during the T cell response are
191 enriched in the memory pool, so we hypothesized that clones with Tex-Prog bias may follow a parallel
192 differentiation trajectory to form cTcm after chronic infection[34]. To test this, we first analyzed scRNA/TCR-
193 seq data to determine if there were Tex-Prog biased clones during chronic infection, similar to the Tex-
194 Prog and cTcm biased clones observed at later time points after clearance. By clustering clones based
195 on intraclonal cluster proportion, we found a subset of clones (n=32) that were ≥50% Tex-Prog (**Extended
196 Data Fig. 4a,b**). Next, to test if Tex-Prog biased clones preferentially formed cTcm, we longitudinally
197 traced clones from the chronic phase of infection to after peripheral viral clearance in the same mice. We
198 sorted PD-1$^+$ Tex subsets (Tex-Int, Tex-KLR, and Tex-Prog) from the blood at 21 dpi, and after peripheral
199 antigen clearance at 100 dpi, we performed TCR-seq of T cell subsets (cTcm, cTem 1, cTem 2, Tex-
200 Prog, and Tex-Term) and compared clonal behaviors between timepoints (**Fig. 2f**, **Extended Data Fig.
201 4c**). We analyzed PD-1$^+$ cells, rather than GP33$^+$ cells, to evaluate T cells with a wider range of TCR
202 avidity for antigen, instead of only high avidity clones that bind tetramer[35]. To validate this system prior
203 to performing longitudinal clone tracing, we first analyzed TCR-seq data from PD-1$^+$ T cell subsets in the
204 spleen and blood of the same mouse at 28 dpi, which demonstrated that clone size and Tex-Prog, Tex-
205 Int, and Tex-KLR phenotype distribution were significantly correlated between tissues (*P*<0.0001),
206 suggesting that blood sampling accurately captures clonal behaviors of splenic Tex at a given time point
207 (**Extended Data Fig. 4c-h**). Of note, and as previously described, there were few Tex-Term present in
208 the peripheral blood, and we observed that splenic Tex-Term frequency showed the highest correlation
209 with Tex-Int frequency in the blood (**Extended Data Fig. 4g,h**; ref[36]).

210   In the longitudinal data, we first replicated the results of the adoptive cell transfer experiments by
211 analyzing clonal relationships between cell subsets at different timepoints. We calculated the subset
212 frequency of each clone at both timepoints and then assessed the correlations of each subset frequency
213 at 21 and 100+ dpi. Strikingly, intraclonal frequency of the Tex-Prog subset at 21 dpi significantly
214 correlated with a clone's cTcm frequency at 100+ dpi (R=0.39 *P*<0.001), supporting the link between the
215 Tex-Prog and cTcm (**Fig. 2g**). In contrast, the intraclonal frequency of Tex-KLR from 21 dpi was
216 significantly correlated with cTem 1 frequency after viral clearance (R=0.43 *P*<0.001), and Tex-Int
217 frequency at 21 dpi was significantly correlated with cTem 2 (R=0.28 *P*<0.001) and Tex-Term (R=0.25

5

218 *P*<0.001) frequency after viral clearance (**Fig. 2g**). Finally, we examined the differentiation patterns of
219 individual clones between time points. We isolated clones that were detected at both timepoints (n=529)
220 and clustered clones based on intraclonal phenotype proportion from the blood at 21 dpi to identify Tex-
221 Prog biased, Tex-KLR biased, Tex-Int biased, and divergent clonal behaviors (**Fig. 2h**). Similarly, we
222 clustered the longitudinally traced clones based on phenotype proportion at 100+ dpi and identified cTcm
223 biased, cTem 1 biased, cTem 2 biased, Tex-Prog biased, Tex-Term biased, and divergent clones (**Fig.**
224 **2h**). To identify the origin of cTcm biased clones, we compared the behavior of each clone at both
225 timepoints and found that approximately 50% of Tex-Prog biased clones (34/69 clones; 50.7% +/-11.9%
226 CI by logistic regression) detected in the blood at 21 dpi became cTcm biased clones after peripheral
227 viral clearance at 100+ dpi (**Fig. 2i**). Conversely, divergent clones detected in the blood, many of which
228 contain Tex-Prog, rarely formed cTcm biased clones (7/113 divergent clones, 5/32 Tex-Prog containing
229 divergent clones; **Fig. 2h**). Similarly, only a small fraction of Tex-Int (36/211 clones) or Tex-KLR (16/136
230 clones) formed cTcm biased clones after viral clearance (**Fig. 2h**). These findings demonstrate that a
231 subset of Tex clones with Tex-Prog bias preferentially gives rise to clonally restricted cTcm, highlighting
232 the role of clonal diversification in the generation of memory cells after clearance of chronic antigen.
233
234 **Shared epigenomic cell states of cTcm and aTcm**
235   Since chronic antigen stimulation can lead to changes in Tex chromatin state that may not be
236 immediately reflected in RNA expression, we asked whether these changes were also observed in
237 cTcm[25,28]. We performed epigenomic profiling of antigen-specific T cell subsets using ATAC-seq to
238 measure the accessibility of *cis*-regulatory elements associated with exhaustion[37]. We sorted GP33^{+}
239 CD8^{+} T cell subsets from the spleen after peripheral LCMV-Cl13 clearance, as well as GP33^{+} Tex
240 populations from LCMV-Cl13 infected mice 28 dpi and GP33^{+} memory T cells after LCMV Arm infection
241 for comparison (**Fig. 3**, **Extended Data Fig. 5a**). We first analyzed the 10,000 most variable open
242 chromatin regions (OCRs; 500bp non-overlapping genomic regions) between samples and performed
243 PCA and clustering, which identified five clusters of samples with global similarities in chromatin
244 accessibility (**Fig. 3a**). Strikingly, cTcm samples clustered exclusively with aTcm, rather than with Tex-
245 Prog from chronic infection, including CD62L^{+} Tex-Prog, which have recently been identified as a more
246 functional population of Tex-Prog (**Fig. 3a**; ref[16]). Similarly, cTem samples clustered with aTem,
247 reinforcing the notion that Tex can differentiate into Tem/Tcm in a parallel manner to acutely stimulated
248 cells after chronic antigen clearance. Tex-Prog that persisted past chronic antigen clearance clustered
249 on their own, and PCA analysis showed that this subset exhibits an intermediate state between Tex-Prog
250 from active infection and Tcm (**Fig. 3a**).
251   We next analyzed the accessibility of OCRs across all samples to identify *cis*-regulatory elements
252 associated with distinct cell states, and linked OCRs to genes based on the nearest transcription start
253 site (TSS; **Fig. 3b,c**; **Supplementary Table 3**; ref[38,39]). Two clusters exhibited chromatin accessibility of
254 effector- (C1; *Klrg1, Zeb2, Tbx21*-associated OCRs) and exhaustion-associated genes (C2; *Tox, Pdcd1,*
255 *Tigit*-associated OCRs), respectively (**Fig. 3b**). The other two clusters (C3, C4) exhibited accessibility of
256 memory-associated genes, with C4 being specifically enriched for Tcm-associated (*Sell, Il7r*) genes, and
257 C3 being enriched for genes expressed by both Tcm and Tex-Prog (*Tcf7, Lef1*; **Fig. 3b**). Notably,
258 compared to other subsets from cleared LCMV-Cl13, cTcm had decreased accessibility for C2
259 exhaustion-related OCRs, which included the exhaustion-specific -23kb *Pdcd1*-associated enhancer and
260 three *Tox*-associated elements (+120kb +109kb +59kb; **Fig. 3c,d**; ref[17,40]). Similarly, cTcm had increased
261 accessibility of C4 Tcm-related OCRs, including a *Tcf7* promoter element (-0.89kb), and *Ccr7* (TSS,
262 +2.5kb)*, Il7r* (TSS, -44kb), and *Lef1*-associated (+2kb, -76.7kb) elements (**Fig. 3c**). To validate
263 differences in exhaustion-associated OCRs, we calculated the number of differentially accessible regions
264 (DARs; Log$_2$FC>1, False Discovery Rate [FDR] <0.01) between Tex-Term and other subsets (**Fig. 3e**;

6

265   **Supplementary Table 4**). We found that cTcm and aTcm had the most DARs when compared to Tex-
266   Term (13,038 and 11,863, respectively), and that cTcm had decreased accessibility of seven *Tox-*
267   *associated cis*-regulatory elements (e.g. TSS, +120kb, +109kb) and the *Pdcd1* -23kb enhancer compared
268   to Tex-Term (**Fig. 3e**). Other populations from cleared LCMV-Cl13 showed fewer DARs versus Tex-Term
269   than cTcm (median=7,888; **Fig. 3e**), suggesting greater epigenomic similarity to the Tex-Term cell state
270   relative to cTcm. Conversely, by comparing cTcm to other cell subsets, we saw fewer DARs versus aTcm
271   (n=146) than other subsets (n>1,100), again supporting the similarity between cTcm and aTcm (**Fig. 3f**).
272   Differences in cTcm and aTcm included increased accessibility of elements associated with *Tox* (+20kb,
273   +109kb) and *Ifi27l2a* (TSS), concordant with gene expression data from scRNA-seq, and decreased
274   accessibility of effector-related gene elements *Klrg1* (+13kb +12kb), which was not seen at the
275   transcriptional level (**Fig. 3f**). Together, this analysis highlights that cTcm exhibit relatively few epigenetic
276   changes from aTcm, compared to other chronic memory cells.

277   To compare our results to the studies that established persistent epigenetic changes in Tex as a
278   result of chronic stimulation (termed "epigenetic scarring"), we generated a set of overlapping OCRs with
279   those identified by Abdel-Hakeem et al[28]. In that study, total P14 T cells were recovered from LCMV-Cl13
280   infected mice and allowed to rest in antigen-free hosts for at least 4 weeks (Tex-Rec). These Tex-Rec
281   were compared with P14 from chronic LCMV-Cl13 infection (Tex) or after clearance of LCMV-Arm
282   (Tmem) by ATAC-seq. We identified 5,781 DARs from this dataset that overlapped with OCRs in our
283   data and compared accessibility of these regions across samples (**Extended Data Fig. 5b**). Indeed, we
284   saw increased accessibility of OCRs associated with Tex epigenetic scarring (e.g. *Tox2* TSS, *Cd101*
285   +8kb, *Stat3* TSS, *Batf* +20kb, *Id2* TSS) in samples from 100+ dpi of LCMV-Cl13 compared to acute
286   memory cells, however, this signature was most pronounced in cTem and Tex-Prog compared to cTcm
287   (**Fig. 3g**). Strikingly, cTcm displayed similar accessibility of these Tex-Rec associated OCRs as cTcm
288   (**Fig. 3g**). Taken together, these data suggest that epigenomic changes that result from chronic
289   stimulation may predominantly persist in cTem and persisting Tex subsets after viral clearance, rather
290   than cTcm, which maintain a chromatin state that is highly similar to aTcm and may underlie *bona fide*
291   memory function.

292

293   **Functional memory recall responses by cTcm**
294   Previous studies have shown that memory-like cells that persist after chronic infection have impaired
295   capacity to expand and differentiate upon recall response[4,27,28]. However, polyclonal memory T cell pools
296   are comprised of individual clones with differential capacity to expand and differentiate upon
297   rechallenge[41–43]. Based on their transcriptional and epigenetic profile, we hypothesized that cTcm biased
298   clones would preferentially respond to rechallenge. To test clonal heterogeneity during rechallenge, we
299   transferred polyclonal CD8$^+$ T cells from mice with cleared LCMV-Cl13 or LCMV-Arm into congenic
300   recipients and rechallenged with LCMV-Arm (**Fig. 4a**). In line with previous studies, bulk T cells
301   transferred from cleared LCMV-Cl13 donors (Cl13:Arm) displayed decreased expansion (FC=16.3
302   *P*=0.0079; **Fig. 4b**) and increased PD-1$^+$ frequency (FC=2.0 *P*=0.0079; **Extended Data Fig. 6b**)
303   compared to cells from cleared LCMV-Armstrong (Arm:Arm) donors by flow cytometry[27,28]. Once we
304   established that this model aligned with previous studies, we expanded the analysis to study the recall
305   response of individual clones. First, we validated that characteristics of clones were replicable between
306   hosts by evaluating expansion and phenotype among clonally-related cells challenged in five separate
307   hosts by scRNA/TCR-seq. Cells from the same clone had significantly correlated clone size ($P<1.1 \times 10^{-5}$;
308   **Fig. 4c**, **Extended Data Fig. 6d**) and gene expression ($P<2.2 \times 10^{-16}$; **Fig. 4c**, **Extended Data Fig. 6e**),
309   compared to randomly generated clones, demonstrating the feasibility of studying clonal differentiation
310   patterns of individual Cl13:Arm T cell clones during a recall response using this model.

311   We next evaluated the clonal expansion of individual clones after transfer and observed an overall
312   decrease in clonal expansion among Cl13:Arm (Median=3.36) cells compared to Arm:Arm cells
313   (Median=7.04; $P<2.2\times10^{-16}$; **Fig. 4d**). Surprisingly, a subset of Cl13:Arm clones (20/261 clones)
314   expanded to the same degree as Arm:Arm clones (≥Arm:Arm median; **Fig. 4d**), suggesting that while the
315   total pool of antigen-specific cells after chronic antigen clearance has impaired recall capacity, there are
316   individual clones that retain functional memory capacity. To determine the origin of these functional
317   chronic antigen-specific clones, we identified clonal behaviors pre-transfer by sorting T cell subsets and
318   performing bulk TCR-seq (**Extended Data Fig. 6f**). Consistent with our prior analysis, we identified five
319   clonal behaviors of Cl13:Arm cells pre-rechallenge by clustering: cTcm bias, Tex-Prog bias, Tex-Term
320   bias, and two cTem bias clusters (**Extended Data Fig. 6f**). We assessed the expansion of clones in each
321   behavior after rechallenge and observed that cTcm biased clones expanded significantly better than
322   Cl13:Arm clones from other pre-transfer behaviors (cTem Bias 1: FC=6.31 $P=1.5\times10^{-6}$, cTem Bias 2:
323   FC=7.75 $P=9.8\times10^{-7}$, Tex-Prog Bias: FC=8.98 $P=0.0036$, Tex-Term Bias: FC=7.17 $P=0.00047$; **Fig. 4e**).
324   Moreover, there was no significant difference in expansion between cTcm biased clones and Arm:Arm
325   clones, including aTcm biased clones, ($P>0.05$; **Fig 4e**; clonal behaviors of Arm:Arm clones determined
326   by the same method as Cl13:Arm; **Extended Data Fig. 6f**), demonstrating the ability of cTcm-based
327   clones to robustly expand upon rechallenge to the same degree as acute memory cells.
328   To further support these findings, we evaluated the recall responses of cTcm *in vivo* using cell transfer
329   experiments. cTcm and other subsets of P14 cells from 100+ dpi of LCMV-Cl13 (cTem, Tex-Prog, and
330   Tex-Term) or P14 aTcm from 50+ dpi of LCMV-Arm were transferred into naive congenic hosts and
331   challenged with LCMV-Arm (**Extended Data Fig. 7a,b**). At 7 dpi, we quantified the expansion of P14
332   cells by flow cytometry and found that there were significantly higher numbers of cTcm-derived cells
333   compared to other chronic memory subsets (Tex-Prog: FC=1.77 $P=0.0104$, cTem: FC=50.6 $P<1\times10^{4}$,
334   Tex-Term: FC=105.1 $P<1\times10^{4}$; **Extended Data Fig. 7c**). Importantly, cTcm expanded and differentiated
335   into KLRG1^{+} effectors to a similar degree as aTcm ($P>0.05$; **Extended Data Fig. 7c,d**), although a
336   significantly increased number of cTcm were PD-1^{+} upon rechallenge compared to aTcm (FC=3.75
337    $P=0.025$; **Extended Data Fig. 7d**). To assess the capacity of individual Cl13:Arm clones to differentiate
338   into effector cells after rechallenge, we analyzed scRNA/TCR-seq (n=47,369 cells total) of transferred
339   CD8^{+} T cells and endogenous GP33^{+} cells from 8 dpi with LCMV-Arm (**Fig. 4f**). scRNA/TCR-seq
340   clustering revealed 10 clusters of cells, which were identified by DEGs (LogFC>0.25; **Fig. 4f**;
341   **Supplementary Table 5**). These included effector cells (Teff; expressing *Zeb2, Klrg1*), memory-
342   precursor effector cells (MPEC; expressing *Tcf7, Ltb*), and Tem (expressing *Cxcr3, Il7r*) clusters, as well
343   as exhaustion-associated clusters, characterized by *Tox* and *Pdcd1* expression along with Teff (*Gzma,
344   Cx3cr1*), Tem (*Cxcr3, Il7r*), or Tex-Term (*Tigit, Lag3, Cd7*) genes (**Extended Data Fig. 7e**). In line with
345   flow cytometry data, the majority of Arm:Arm and endogenous GP33^{+} cells were in Tem and Teff clusters,
346   while most Cl13:Arm cells were in exhausted clusters (**Fig. 4g**, **Extended Data Fig. 7f**). However, 32.3%
347   of Cl13:Arm cells did not appear phenotypically exhausted and were in Teff and Tem clusters (**Fig. 4g**).
348   At the clonal level, we found a subset of clones (n=39/187) that had a low proportion of cells in the
349   exhaustion-associated clusters (**Fig. 4h**). We assessed the origins of these clones and determined that
350   the probability of cTcm biased clones becoming >50% exhausted (38.5% +/-26.4% CI by logistic
351   regression) was lower than clones from other Cl13:Arm behaviors (>75% probability; **Fig. 4i**). Similarly,
352   cTcm biased clones had lower expression of genes including *Tox*, *Pdcd1*, and *Lag3*, relative to other
353   Cl13:Arm clones (**Extended Data Fig**). Next, we tested the ability of individual clones to upregulate
354   effector related genes (including *Klrg1, Ccr2, Ly6c2*; **Supplementary Table 7**) and found that some
355   clones had a significantly higher effector module score than the total population of Cl13:Arm cells (**Fig.
356   4j**). Overall, 38.5% of cTcm biased clones had a significantly higher effector module score than the total
357   population of Cl13:Arm cells, a higher frequency than any other clone behavior (**Fig. 4j,k**). As validation,

8

358 we observed increased expression of individual genes (*Klrg1, Ccr2, Ly6c2*) in the effector gene module
359 among cTcm clones compared to other Cl13:Arm clones (**Extended Data Fig 7g**). Taken together, these
360 data suggest that cTcm biased clones can robustly expand and differentiate into effector cells upon
361 rechallenge.

362   Finally, to assess whether increased clonal expansion and differentiation enables pathogen clearance
363 by cTcm, we transferred P14 T cell subsets into TCRα$^{-/-}$ mice, which lack endogenous CD4^{+} and CD8^{+} T
364 cells, and challenged with LCMV-Arm. Transfer of either aTcm or cTcm led to significant reduction in
365 LCMV viral burden compared to untreated controls (aTcm: FC=2.22 *P*=0.0017; cTcm: FC=3.35
366 *P*<0.0001), while other subsets of CD8^{+} chronic memory cells had no impact on viral burden (*P*>0.05;
367 **Fig. 4I**). Importantly, there was no significant difference between cTcm and aTcm (*P*>0.05), further
368 demonstrating the functional recall response of cTcm (**Fig. 4I**). Together, these findings demonstrate that
369 the expansion and differentiation of cTcm biased clones upon rechallenge enables protective immunity.
370

371 **αPD-L1 treatment expands cTcm biased clones**

372   Since Tex-Prog preferentially respond to ICB and cTcm are derived from Tex-Prog biased clones, we
373 assessed the impact of ICB on cTcm. Specifically, we tested whether ICB: (1) impacted the durability of
374 cTcm, and (2) led to the expansion of cTcm biased clones[10,15,16]. To test this, we treated LCMV-Cl13
375 infected mice with a monoclonal antibody blocking PD-L1 (αPD-L1), the ligand for PD-1 (**Fig. 5a**). As
376 shown previously, αPD-L1 treatment led to significant expansion of GP33^{+} cells during the chronic phase
377 of infection (FC=1.62 *P*=0.028; **Fig. 5b**); however, there were no significant (*P*>0.05) differences in GP33^{+}
378 frequency or count after viral clearance between groups (**Fig. 5b**, **Extended Data Fig. 8a**; ref[44]). We
379 performed scRNA/TCR-seq on splenic GP33^{+} T cells at 100+ dpi to assess if αPD-L1 impacted the
380 frequency or gene expression profiles of chronic memory cells and again found no significant changes in
381 subset frequencies of chronic memory T cells after αPD-L1 treatment, compared to PBS-treated controls
382 (**Fig. 5c**, **Extended Data Fig. 8b-d**, **Supplementary Table 6**), which we further validated with flow
383 cytometry (**Extended Data Fig. 8e**). Within cell clusters, gene expression was also highly correlated
384 (R>0.9, *P*<0.001) between groups and there were less than 10 DEGs between groups across all clusters
385 (**Extended Data Fig. 8f,g**). Finally, we assessed if clonal behaviors were altered by αPD-L1 treatment,
386 and found all clonal behaviors, including cTcm biased clones, in αPD-L1 treated mice (**Fig 5d**).

387   Given that cTcm preferentially differentiate from Tex-Prog biased clones, we hypothesized that αPD-
388 L1 treatment may selectively expand clones that form cTcm. Moreover, ICB acts by expanding pre-
389 existing Tex-Prog clones as well as by priming new clones, so we tested the impact of both mechanisms
390 of action on the formation of cTcm[45,46]. To evaluate the contribution of αPD-L1 mobilized clones to the
391 cTcm pool, we performed longitudinal bulk TCR-seq on T cell subsets from blood pre- and post-αPD-L1
392 treatment (Tex-Prog, Tex-Int, and Tex-KLR), and at a memory timepoint (Tcm, Tem 1, Tem 2, Tex-Prog,
393 and Tex-Term; **Fig. 5e**, **Extended Data Fig. 4c**). Again, we did not restrict analysis to GP33^{+} clones,
394 because T cells with low avidity TCRs preferentially respond to ICB[47]. To assess clonal trajectories over
395 time, we adapted an existing analytical framework (Cyclone; ref[48]) to determine longitudinal trajectories
396 based on the clustering of pairwise correlations of clone subset frequencies at each timepoint (**Fig. 5f**).
397 This approach yielded eight clonal trajectories, including clones that contracted over time (Trajectory 1-
398 4) and clones that expanded after the treatment period (Trajectory 5-8; **Fig. 5f,g**). Expanding clonal
399 trajectories included clones not present before treatment, which could either be *de novo* primed clones
400 or clones present at low/undetectable frequencies prior to αPD-L1. Utilizing longitudinal phenotype
401 information, we identified clones that phenotypically transitioned from Tex-Int and Tex-KLR to cTem
402 (Trajectories 1,2,5,8) as well as clones that transition from Tex-Prog that resulted in cTcm (Trajectories
403 3,4,6,7; **Fig 5h**). We assessed which longitudinal trajectories could lead to clones with a significant bias

9

404   toward cTcm (*P*<0.05 hypergeometric test), and found that cTcm biased clones could arise from all
405   longitudinal trajectories (**Fig 5i**), as shown in earlier clone tracing experiments. Importantly, αPD-L1
406   treatment yielded more cTcm biased clones, primarily from clones in Trajectory 7 (FC=2.97) and few
407   cTcm biased clones from Trajectory 6 (FC=41.7; **Fig. 5j**). Trajectory 7 was enriched for clones that were
408   small or undetected pre-treatment, evenly spread across phenotypes at d35, further expanded from 35
409   dpi to 100 dpi, and primarily formed majority cTcm (**Fig. 5g,h**). Trajectory 6 clones were generally >70%
410   Tex-Prog at 35 dpi, formed cTcm at 100+ dpi, and contracted from 35 to 100+ dpi (**Fig. 5g,h**). Among all
411   clone trajectories, Trajectory 7 was the most enriched in the αPD-L1 group compared to control (80.2%
412   +/-3.48% CI in αPD-L1 by logistic regression), while Trajectory 6 was depleted (28.4% +/-4.47% CI in
413   αPD-L1; **Fig. 5j**). These data suggest that αPD-L1 ICB may drive the proliferation and differentiation of
414   previously unexpanded T cell clones that contribute to the cTcm pool after antigen clearance.
415

Discussion

417   Here, we describe a clonally restricted subset of Tex that maintains the phenotypic plasticity to form
418   functional long-lived memory T cells. We utilized clonally resolved phenotypic profiling of the polyclonal
419   T cell response to uncover multiple differentiation trajectories of T cells that persist following chronic
420   antigen clearance. Specifically, cTcm preferentially differentiated from Tex-Prog biased clones, and cTem
421   developed from more differentiated effector-like Tex-Int and Tex-KLR clones, mirroring analogous
422   memory differentiation trajectories after acute infection. cTcm exhibited transcriptional and epigenetic
423   states that were nearly identical to aTcm, and they were able to robustly expand, differentiate into effector
424   T cells, and clear secondary viral infections to the same extent as aTcm.
425   Prior studies have shown that T cells maintain exhaustion-related epigenetic changes or "scars" from
426   chronic stimulation that impair their subsequent recall response[25,27,28]. Our data are consistent with this
427   finding as we observe that the majority of Tex-derived cells–including cTem and Tex subsets–maintain
428   chromatin accessibility of exhaustion-associated loci after clearance of chronic viral infection, and
429   accordingly, are unable to respond to rechallenge. However, we find that a subset of Tex-Prog clones is
430   able to avoid this epigenetic fate and lead to cTcm. Since cTcm are a relatively small fraction of the total
431   antigen-specific T cell pool after viral clearance, we suspect that the functional response and genomic
432   signatures of these clones may be masked in population-level analyses. Previous work has suggested
433   that the preservation of Tex-Prog in the setting of chronic antigen can be maintained by cell extrinsic
434   factors, including the sequestration of T cells in low antigen density spatial niches[9,36,49,50]. Our results may
435   support and extend this concept, since chronic LCMV infection can persist long-term locally in many
436   organs even after peripheral clearance; therefore, the generation of Tex-Prog biased clones and cTcm
437   may require stable lymphoid niches that preserve memory plasticity by avoiding antigen exposure and
438   TCR stimulation[1]. In line with this concept, low TCR signal strength–via low avidity or decreased dendritic
439   cell activation–has been shown to promote a stem-like Tex cell state, while high avidity TCRs
440   preferentially form Tex in both tumors and chronic infection[11,47,50–53]. This model is further supported by
441   the robust expansion of cTcm clones after αPD-L1 treatment, since low avidity clones are preferentially
442   engaged by ICB[47].
443   Our findings also complement recent studies that demonstrate parallel differentiation trajectories of
444   stem-like T cells at the earliest stages of chronic and acute infection[54,55]. These studies have shown that:
445   (1) T cells with high TCR avidity for antigen preferentially differentiate into Tex-Prog during acute
446   stimulation, and (2) stem-like T cells early in infection are nearly identical in both viral challenge settings,
447   which may represent an anticipatory mechanism to prepare the host for different infection outcomes[54,55].
448   Our work extends this model and demonstrates that a similar parallel exists at memory time points after
449   pathogen clearance, where some Tex-Prog-derived cells maintain durable epigenetic adaptations to
450   chronic stimulation, while a clonally-distinct subset of Tex-Prog-derived cells form cTcm that can robustly

10

451 respond to acute secondary rechallenge, which may represent a similar anticipatory evolutionary
452 adaptation for a broad range of secondary infection outcomes.
453   Finally, the expansion of cTcm biased clones upon αPD-L1 treatment may provide a mechanistic
454 explanation for several clinical observations. First, tumor-specific T cell clones that expand after αPD-
455 (L)1 treatment in patients can be found in the blood and persist for years after therapy[24,56]. However,
456 since these clones were exhausted in the tumor microenvironment, it has been unclear if they could
457 contribute to the memory response and promote long-term survival, which can last for over a decade[57].
458 Our prior work demonstrated that the presence of tumor-specific Tex-Prog in tumor-draining lymph nodes
459 of these patients was associated with a greater likelihood of long-term persistence in the blood, and our
460 current study bridges this gap and suggests that a fraction of the Tex-Prog population may lead to the
461 differentiation of *bona fide* memory cells long-term[24]. Second, αPD-(L)1 ICB enhances vaccine induced
462 antitumor responses, which may augment long-term survival[58,59]. Our data suggest that this may be
463 driven by the invigoration of novel and lowly expanded T cell clones, which contribute to the functional
464 memory T cell repertoire and support long term-immunity. Finally, our results support growing evidence
465 that clonal responses to ICB can be derived from two sources: (1) clonal reinvigoration or revival, where
466 ICB leads to differentiation of pre-existing clones, and (2) clonal replacement, where ICB leads to *de*
467 *novo* priming of naive T cell clones[45,46]. We find that both pre-existing and novel clones comprise the
468 cTcm pool. Pre-existing ICB-activated clones produce differentiated Tex immediately following treatment,
469 while also maintaining cells in their capacity to form memory. In addition, ICB leads to the expansion of
470 novel clones that form cTcm, which may be enriched for low avidity clones that are primed due to
471 increased TCR signaling with ICB. Altogether, these findings underscore the capacity of select exhausted
472 T cell clones to maintain phenotypic plasticity and transition to functional memory cells, providing a
473 foundation for future interventions to enhance immune memory to chronic infections and cancer.

474   **Figures**

475

476   ***Figure 1: Tcm arise after the clearance of chronic viral infection.***

477   (a-f) scRNA/TCR-seq of GP33$^+$, GP33$^+$ CD62L$^+$, and GP33$^+$ CD62L$^-$ CD8$^+$ T cells sorted from the spleen

478   at various timepoints after LCMV-Cl13 or LCMV-Arm. (a) Experimental schematic: LCMV-Arm and

479   LCMV-Cl13 viral burden are graphically illustrated as shaded regions. (b) UMAP of all scRNA-seq cell

480   profiles colored by cluster. (c) Differentially expressed genes per cell cluster. (d) UMAP of cells from each

481   group colored by cluster. (e) Pearson correlation of PCs 1-30 between cleared LCMV-Cl13 clusters and

482   chronic LCMV-Cl13 or LCMV-Arm clusters (Bonferonni corrected *P* values). (f) Number of differentially

483   expressed genes (DEGs) between cTcm or cTem and cell subsets from chronic LCMV-Cl13 or LCMV-

484   Arm. (a-f) n=8 cleared LCMV-Cl13, n=5 LCMV-Arm, n=8 chronic LCMV-Cl13. Data are pooled from two

485   experiments. (g) Flow cytometry gating scheme for T cell subsets 100+ dpi with LCMV-Cl13 (gated on

486   live CD8$^+$). (h) Cell subset frequency of GP33$^+$ cells 100+ dpi LCMV-Cl13. (i,j) CD127, TCF-1, PD-1, and

12

487   TOX expression among GP33$^+$ cell subsets from 100+ dpi LCMV-Cl13 or controls (aTcm LCMV-Arm
488   100+ dpi; Tex-Prog LCMV-Cl13 21 dpi). (g-j) Data shown as mean +/- SD. n=6 LCMV-Cl13 -100+ dpi,
489   n=5 LCMV-Arm, n=4 LCMV-Cl13 21 dpi. Representative experiment of at least two independent
490   experiments. *P* values calculated by Mann-Whitney U Test. (k) *In vitro* cytokine production by GP33$^+$
491   subsets following 18 hour stimulation with PMA/Ionomycin. n=3-5 replicates per group. Cells pooled from
492   multiple mice: n=11 LCMV-Cl13 -100+ dpi, n=4 LCMV-Arm 100+ dpi, n=6 LCMV-Cl13 30 dpi.
493   Significance for each cytokine are shown versus cTcm, calculated by DESeq2. (a-k)*=*P*<0.05, **=*P*<0.01,
494   ***=*P*<0.001, ns=*P*>0.05.
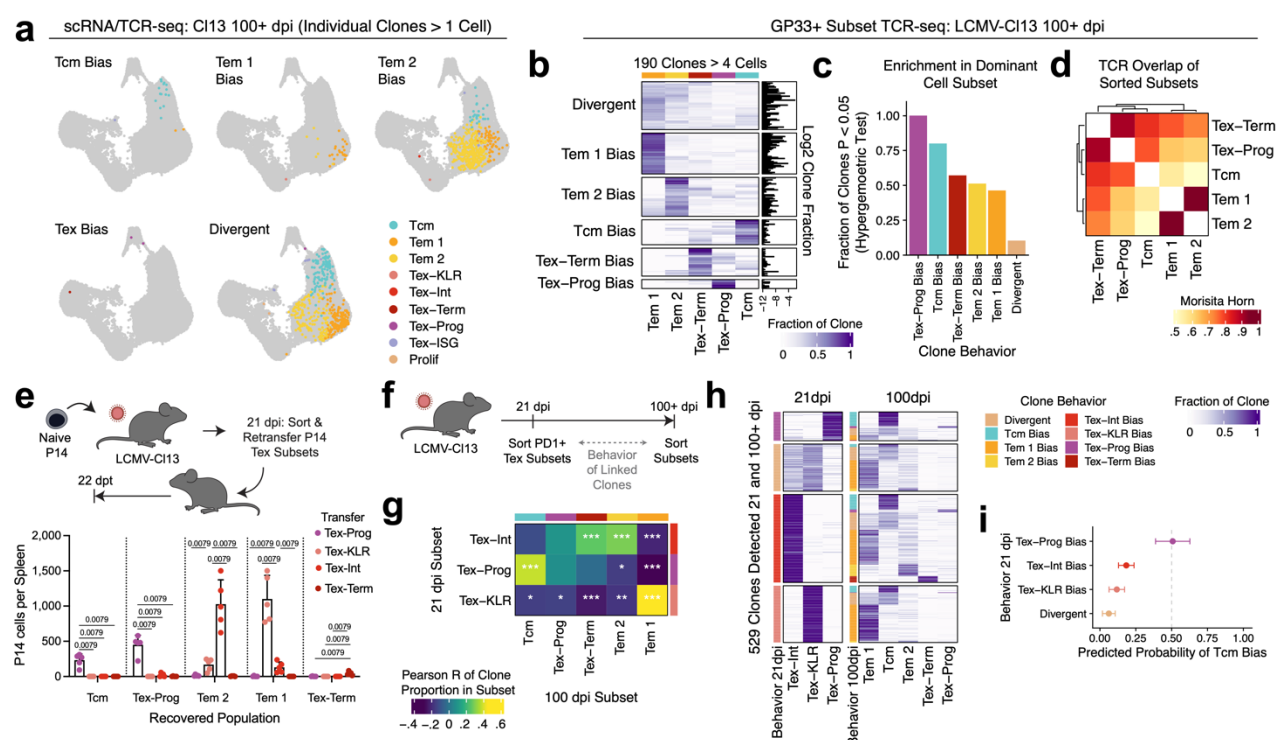
Figure 2: Chronic Tcm originate from Tex-Prog biased clones.

(a) Representative clones of GP33+ CD8+ T cells from scRNA/TCR-seq. Clones are labelled based on k-means clustering of phenotype proportions among all clones from LCMV-Cl13 100+ dpi. See **Extended Data Fig. 3a**. (b-d) Bulk TCR-seq of GP33+ subsets isolated 100+ dpi with LCMV-Cl13 (n=3 mice). (b) Phenotype distribution of individual TCR clones across subsets, grouped by clonal behavior determined by k-means clustering. (c) Fraction of clones with statistically significant enrichment ($P<0.05$ Hoechberg corrected hypergeometric test) for the clone's dominant cell subset. (d) Morisita-Horn TCR overlap index of sorted subsets from bulk TCR-seq. (e) Subsets of exhausted P14 were isolated from LCMV-Cl13 infected mice 21 dpi and 4.5×10^4 cells were transferred into infection free secondary hosts. Flow cytometry quantification of P14 of cell subsets was performed 22 days post transfer (dpt). Bars show mean + standard deviation. n=5 mice per group. Representative experiment of two independent experiments. *P* values calculated by Mann-Whitney U Test. (f-i) T cell clones from LCMV-Cl13 infected mice were subset sorted from the blood 21 dpi and spleen 100+ dpi, and clonal behaviors were analyzed across timepoints by TCR-seq. (g) Pearson correlation of clone frequency in each subset between timepoints (Bonferonni corrected *P* values). (h) Phenotype distribution of individual TCR clones grouped by clonal behavior at 28 dpi and 100+ dpi. Color bars indicate clone behavior at each timepoint. (i) Probability of clones within different exhausted clone behaviors transitioning to cTcm bias after peripheral viral clearance. Probability +/- 95% CI calculated by logistic regression. (f-i) n=8 mice. (a-i)*=$P<0.05$, **=$P<0.01$, ***=$P<0.001$, ns=$P>0.05$.
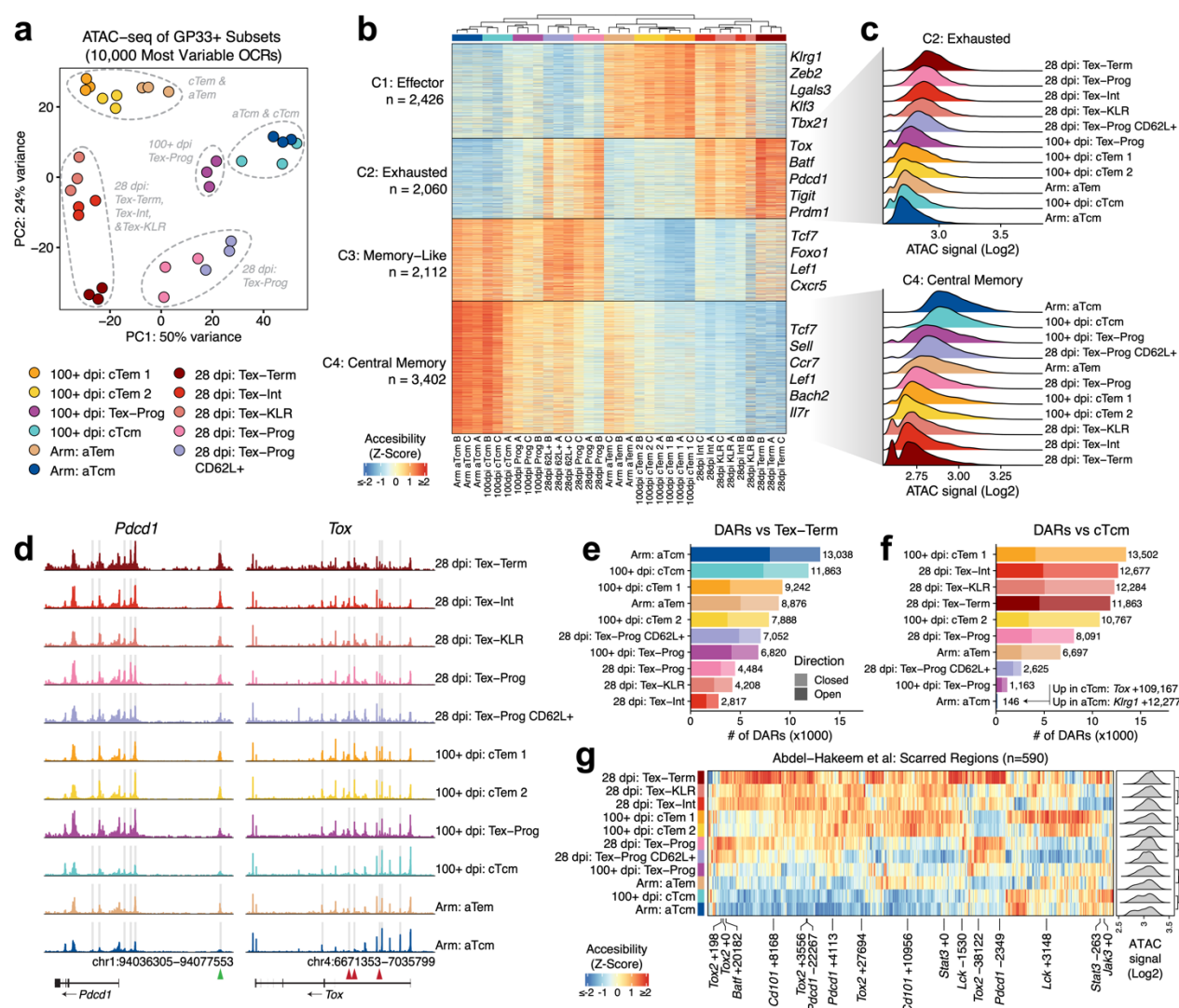
Figure 3: Chronic Tcm and acute Tcm have a shared epigenomic profile.
ATAC-seq was performed on sorted subsets of GP33^{+} CD8^{+} T cell subsets from spleens of mice infected with LCMV-Cl13 (28 or 100+ dpi) or LCMV-Arm (100+ dpi). (a) PCA of top 10,000 most variable open chromatin regions (OCRs). Dotted lines show k-means clustering of samples based on accessibility of top 10,000 OCRs. (b) Accessibility of top 10,000 OCRs among samples. OCRs are clustered by k-means clustering. (c) Accessibility of OCRs in C2 (exhaustion-specific) or C4 (central memory-specific) across groups. (d) Genome tracks for *Pdcd1* and *Tox* across groups. Shaded boxes show the top 10,000 OCRs. Green arrow marks -23kb *Pdcd1* enhancer. Red arrows denote *Tox* OCRs in exhaustion-specific C2. (e,f) Number of differentially accessible regions (DARs) between indicated cells and Tex-Term (e) or cTcm (f). (g) Accessibility of OCRs corresponding to epigenetically scarred regions from ref[28] across samples. (a-g) Each sample is a pool of 2-4 mice. n=3 pools per group.

15

527

Figure 4: Chronic Tcm are functional upon rechallenge.

528   (a-k) 2×10^5 polyclonal CD45.1^{+} CD8^{+} T cells from LCMV-Arm or LCMV-Cl13 infected mice 100+ dpi were
530   transferred into congenic hosts and challenged with LCMV-Arm. Clonal behaviors of cells pre-rechallenge
531   determined by TCR-seq of sorted subsets (**Extended Data Fig. 6f**), and transferred cells were analyzed
532   by scRNA/TCR-seq from the spleen 8 dpi. (b) Quantification of total and GP33^{+} transferred T cells per
533   group. Data shown as mean+/-SD. *P* values calculated by Mann-Whitney U Test. (c) Pearson correlation
534   of (left) clone sizes of clones between hosts and (right) gene expression PCs 1-30 of clonal sisters within
535   the same host or in other hosts. *P* values calculated by Mann-Whitney U Test. (d-e) Clonal expansion of
536   individual clones from (d) indicated donor or (e) clones from different pre-transfer clonal behaviors. *P*
537   values calculated by Mann-Whitney U Test. (f, g) UMAP scRNA-seq profiles of cells 8 dpi colored by cell
538   cluster from (f) all cells or (g) indicated group. (h) Cluster distribution of cells 8 dpi of individual Cl13:Arm
539   clones (n>4 cells) grouped based on pre-rechallenge behavior. (i) Probability of clones from different pre-
540   rechallenge behaviors becoming exhausted clones at 8 dpi (>50% in Exh Teff, Exh Tem, Exh Term
541   clusters). Probability +/- 95% CI calculated by logistic regression. (j) Effector module score of cells from
542   individual Cl13:Arm   clones (n>4 cells). *P* values compare individual clones to total distribution of
543   Cl13:Arm cells by Benjamini-Hochberg corrected Mann-Whitney U test. (k) Frequency of Cl13:Arm clones
544   in each behavior with effector score distributions significantly above or below the total Cl13:Arm
545   distribution. (a-k) n=5 mice/group. (l) Viral burden in the spleen of TCRα^{-/-} mice 7dpi after transfer of 1×10^4
546   subset sorted P14 from LCMV-Cl13 100+ dpi or aTcm from LCMV-Arm 30+ dpi and subsequent LCMV-
547   Arm challenge. n=10 no transfer, n=6 aTcm, n=9 cTcm, n=7 Tex-Prog, n=9 cTem, n=2 Tex-Term. Data

548   pooled from two experiments. *P* values calculated by Mann-Whitney U Test. (a-l) Boxplots show Median,
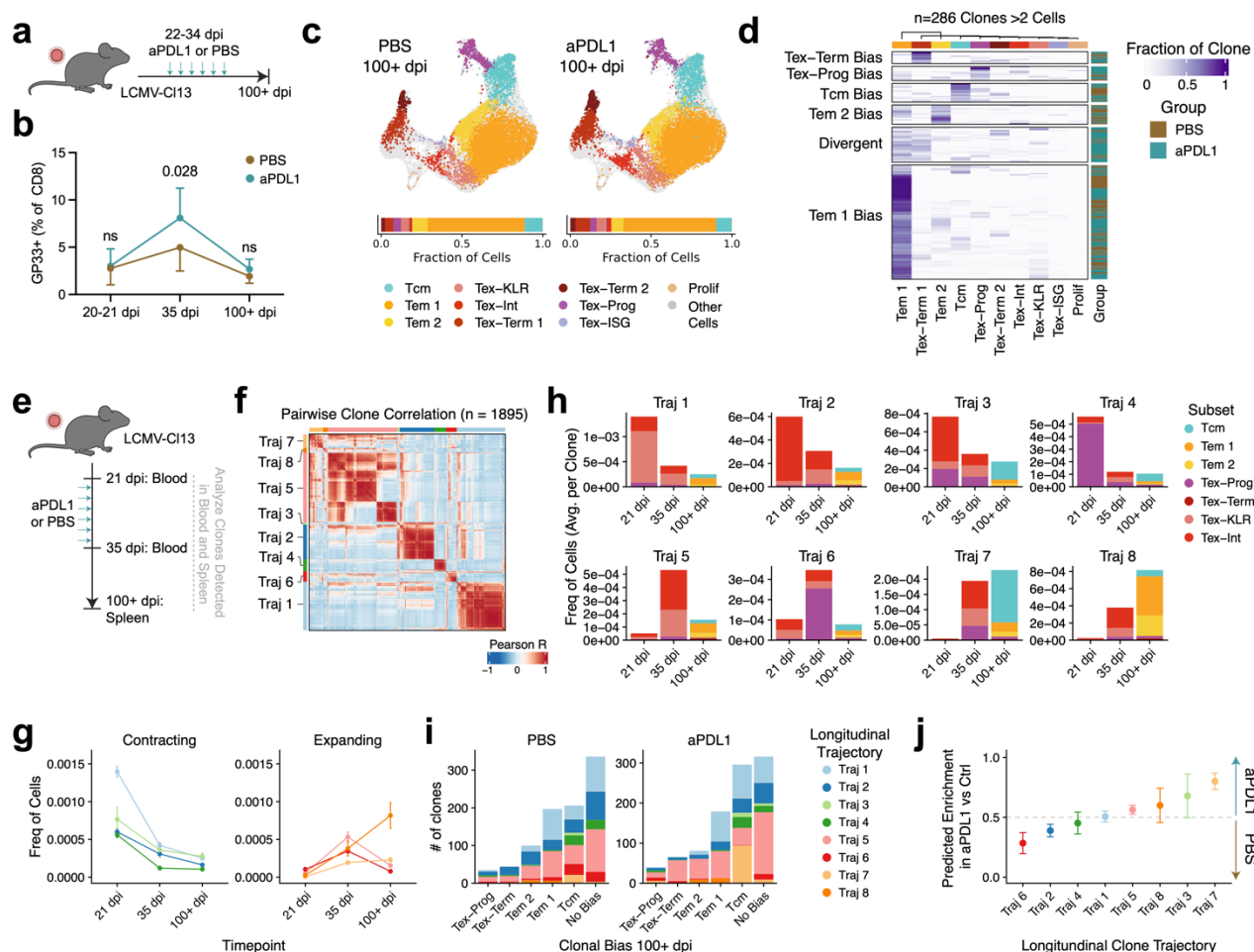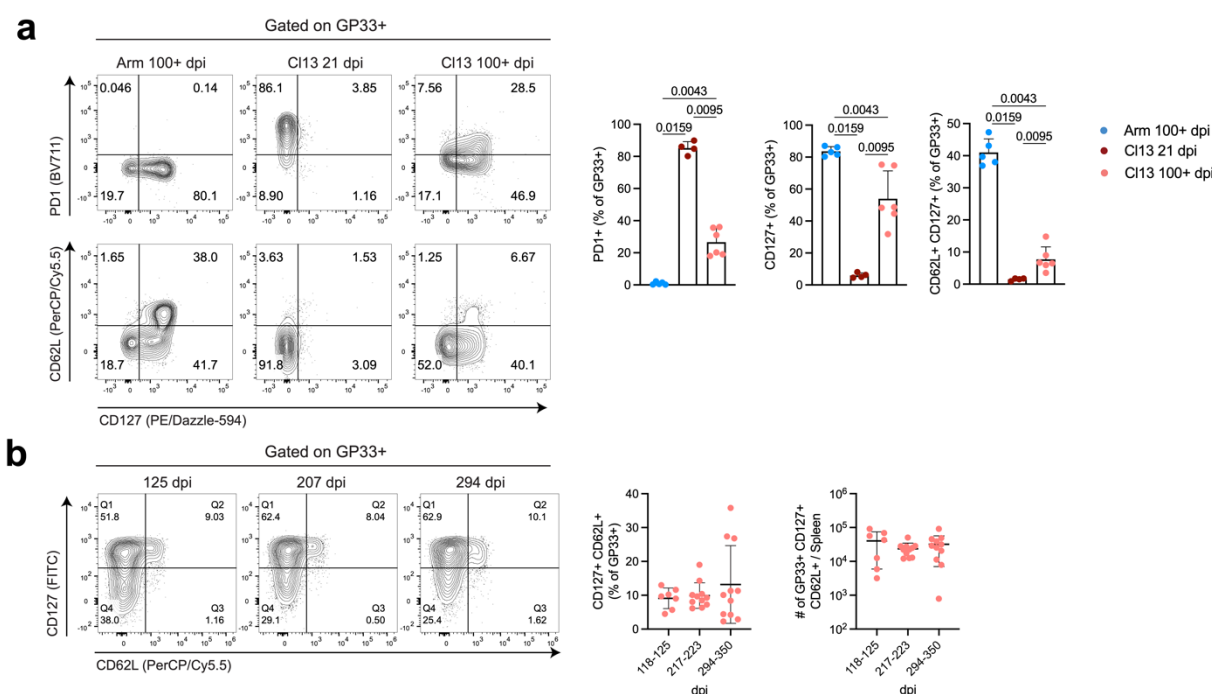549   IQR, and 1.5xIQR. Barplots show mean+/-SD. *=*P*<0.05, **=*P*<0.01, ***=*P*<0.001,ns=*P*>0.05.
550

Figure 5: αPD-L1 treatment expands chronic Tcm biased clones.

(a) Mice were infected with LCMV-Cl13 and treated with αPD-L1 from 22 to 34 dpi. (b) Flow cytometry of GP33+ cell frequency from blood (pre-treatment; 20-21 dpi and post-treatment; 35 dpi) or spleen (100+ dpi). Mean +/- SD. n=12 mice per group from two independent experiments. *P* values calculated by Mann-Whitney U Test. (c-d) 100+ dpi, scRNA/TCR-seq was performed on GP33+ cells from the spleen and integrated with data from **Fig. 1**. (c) Cells from PBS or αPD-L1 treated mice colored by cell cluster. Cells in grey are from other datasets. (d) Phenotype distribution of individual TCR clones across subsets, grouped by clonal behavior determined by k-means clustering. (c-d) n=4 PBS mice , n=5 αPD-L1 mice. (e-j) Cell subsets were sorted from the blood (21 and 35 dpi) or spleen (100+ dpi) of LCMV-Cl13 infected mice treated with PBS or αPD-L1. Bulk TCR-seq was used to trace clonal differentiation across timepoints. (f) Pairwise correlations of clone subset frequencies at each timepoint. Common longitudinal trajectories (Traj) were identified by clustering based on correlations. (g) Clone size of clones in each longitudinal trajectory over time. Plot shows mean +/- SEM. (h) Average subset frequency (of all CD8+ T cells) for clones in each trajectory at different timepoints. (i) Number of clones per group that result in clones biased towards each phenotype at 100+ dpi. Bias determined by *P*<0.05 by hypergeometric test with Hochberg correction. (j) Enrichment of clonal trajectories in αPD-L1 group vs PBS group. Probability +/- 95% CI calculated by logistic regression. (e-j) n=8 PBS mice, n=7 αPD-L1 mice.

18

Extended Data Figures

Extended Data Figure 1: scRNA/TCR-seq categorization of GP33⁺ cells after peripheral LCMV-Cl13 clearance.

(a) Viral burden in the spleen of naïve mice or mice infected with LCMV-Cl13 (22 or 100+ dpi) or LCMV-Arm (22 dpi). Lines show median. Numbers show the fraction of mice with detectable viral load. *P* value calculated by Mann-Whitney U Test. n=3 naïve, n=5 LCMV-Arm, n=5 LCMV-Cl13 22 dpi, n=10 LCMV-Cl13 100+ dpi. (b,c) Sorting scheme (b) and representative post-sort purity (c) for scRNA/TCR-seq. (d) (left) scRNA-seq UMAP of cells sorted from each timepoint colored by sort. (right) Cell cluster distribution from individual samples. (e) Exhaustion module score of all cells (left) and cells from select clusters in each group. Horizontal lines show the median.

Extended Data Figure 2: Flow cytometry of CD62L$^+$ CD127$^+$ Tcm after peripheral clearance of LCMV-Cl13.

(a) Flow cytometry of PD-1, CD127, and CD62L among GP33$^+$ CD8$^+$ T cells in the spleen. n=6 LCMV-Cl13 -100+ dpi, n=5 LCMV-Arm, n=4 LCMV-Cl13 21dpi. Representative experiment of multiple independent experiments. *P* values calculated by Mann-Whitney U Test. (b) Quantification of CD127$^+$ CD26L$^+$ GP33$^+$ cells at indicated timepoints after LCMV-Cl13 infection. n=7 118-125 dpi, n=11 217-223 dpi, n=11 294-350 dpi. Data pooled from two independent experiments. (a,b) Data shown as mean+/- SD.
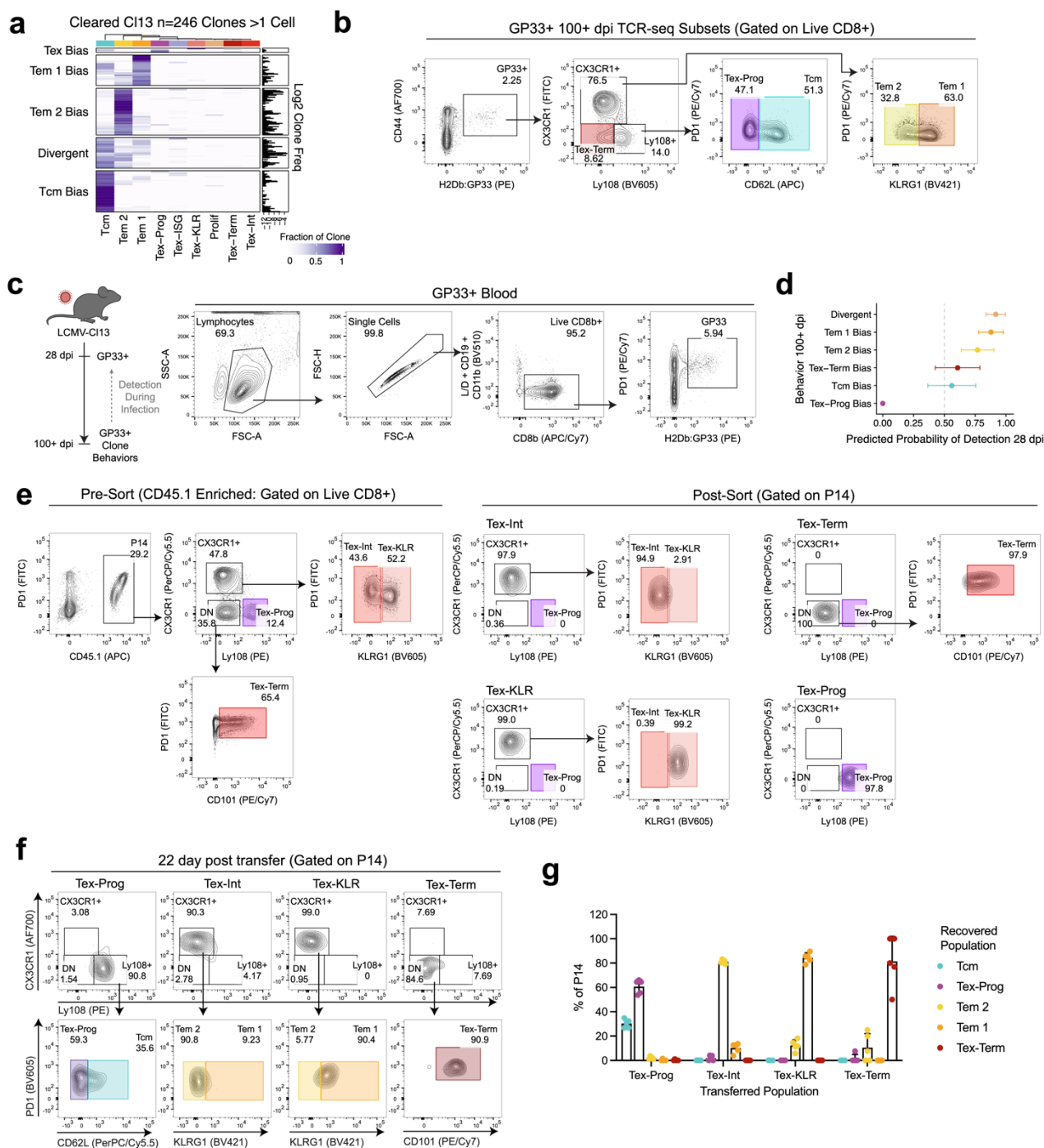
589
Extended Data Figure 3: cTcm are derived from Tex-Prog.
(a) Custer distribution of individual expanded clones from scRNA/TCR-seq from 100+ dpi LCMV-Cl13. Clones are grouped by clonal behavior determined by k-means clustering. (b) Gating scheme for bulk TCR-seq at 100+ dpi. (c,d) Detection of GP33$^+$ clones in blood 28dpi. Clonal behaviors of GP33$^+$ were determined by TCR-seq 100+ dpi (**Fig. 2b**) and detection during infection was tested by TCR-seq of blood GP33$^+$ cells 28 dpi. (d) Probability of clones from different behaviors being detected in blood at 28 dpi. Probability +/- 95% CI calculated by logistic regression. (e-g) 4x10^3 naive CD45.1$^+$ P14 T cells were transferred into congenic primary hosts infected with LCMV-Cl13. Subsets of exhausted P14 cells were isolated and 4.5x10^4 cells were transferred into infection free secondary hosts. After 22 days, cells were isolated and assessed by flow cytometry. (e) Sorting scheme (left) for exhausted P14 subsets and (right)

21

600   sort purity. (f,g) Representative flow cytometry (f) and (g) quantification of cells recovered in secondary
601   hosts 22 days post transfer. Data shown as mean+/-SD. n=5 mice per group. Representative experiment
602   of two independent experiments. *P* values calculated by Mann-Whitney U Test.
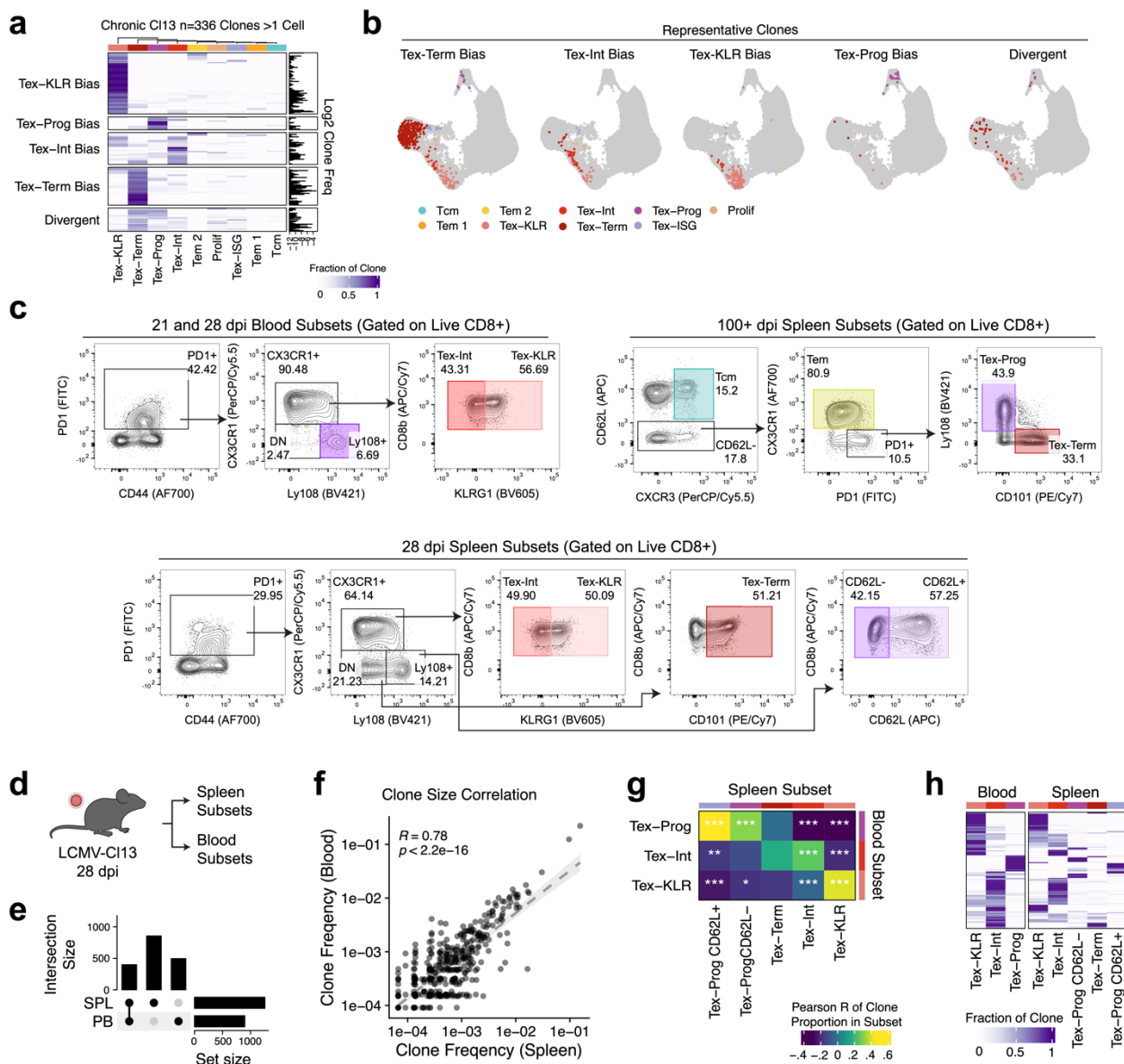
Extended Data Figure 4: Presence of Tex-Prog biased clones in chronic infection and model validation for longitudinal clone tracing.

(a,b) scRNA/TCR-seq of T cell clones from 21-26 dpi LCMV-Cl13. (a) Custer distribution of individual expanded clones from scRNA/TCR-seq. Clones are grouped by clonal behavior determined by k-means clustering. (b) Representative clones from each behavior. (c) Gating schemes for longitudinal bulk TCR-seq studies. (d-h) PD-1+ exhausted cell subsets were sorted from the blood of an LCMV-Cl13 infected mouse 28 dpi. (e) Upset plot of clones detected in the spleen, blood, or both organs. (f) Pearson correlation of total clone frequency in the blood and spleen. (g) Pearson correlation of clone frequency in each subset between organs. Significant correlations by Pearson correlation are highlighted (Bonferonni corrected *P* values: *=*P*<0.05, **=*P*<0.01, ***=*P*<0.001). (h) Phenotype distribution of clone frequency of shared clones in blood or spleen.

615

Extended Data Figure 5: ATAC-seq gating schemes and analysis of overlapping OCRs with Abdel-Hakeem et al.

(a) Gating schemes for ATAC-seq. (b) Accessibility of OCRs corresponding to regions identified in ref[28] across samples.
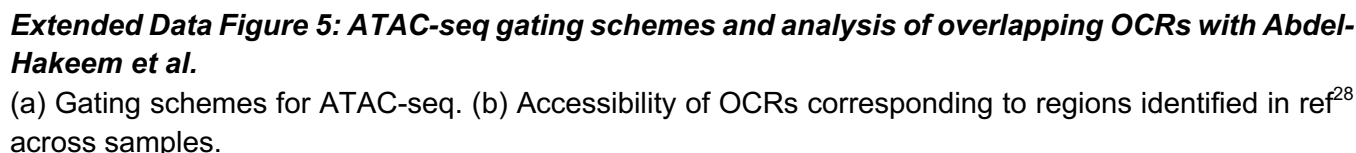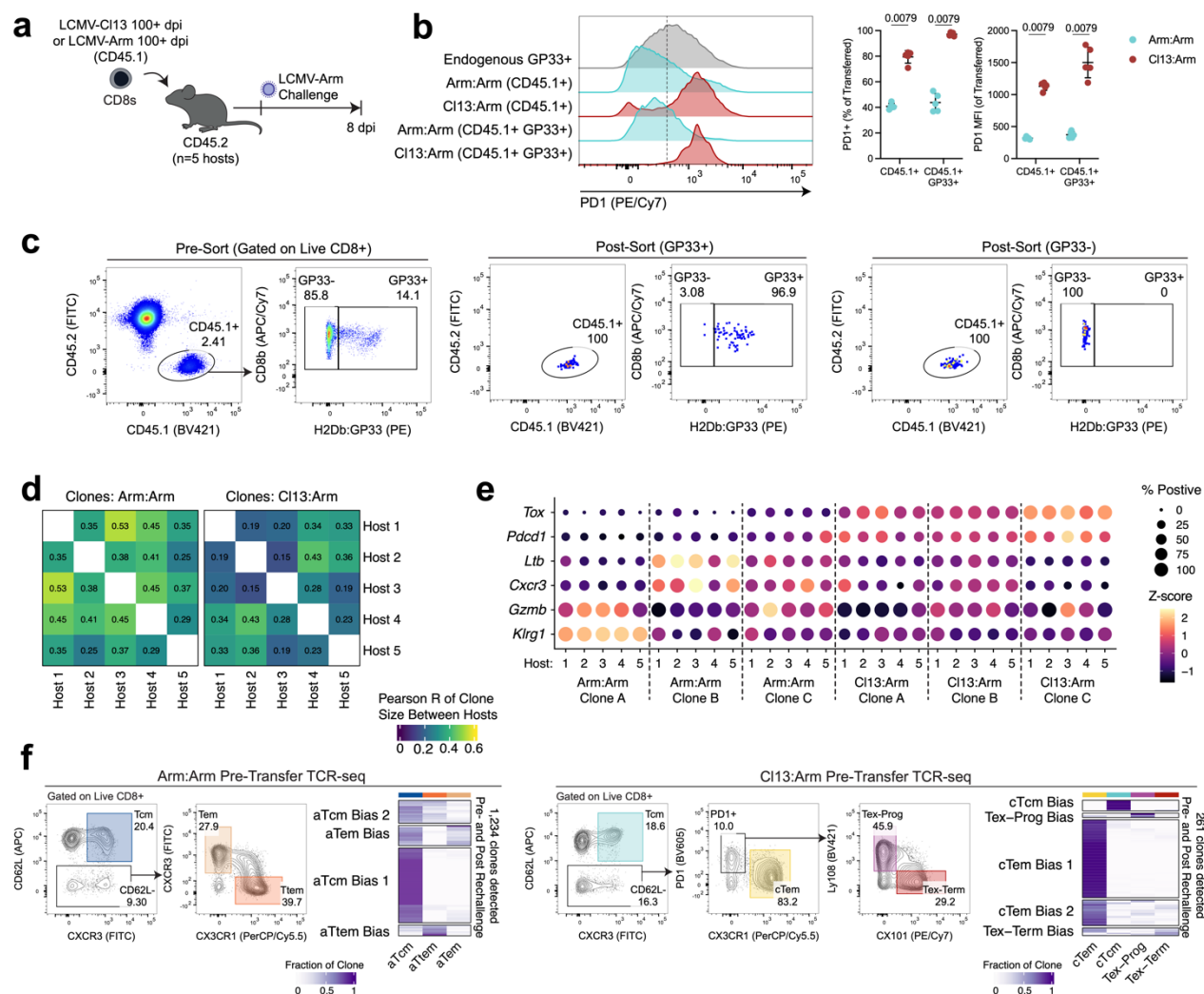
Extended Data Figure 6: Polyclonal rechallenge of CD8+ T cells from 100+ dpi LCMV-Arm or LCMV-Cl13.

(a-f) 2x10^5 polyclonal CD45.1+ CD8+ T cells from LCMV-Arm or LCMV-Cl13 infected mice 100+ dpi were transferred into congenic hosts and challenged with LCMV-Arm. (b) PD-1 expression among transferred CD45.1+, CD45.1+ GP33+, or endogenous CD45.2+ GP33+ T cells at 8 dpi. (c) Sorting scheme and purity for scRNA/TCR-seq 8 dpi. (d) Pearson of clone sizes between individual hosts. (e) Expression of Tex (*Tox, Pdcd1*), Tem (*Ltb, Cxcr3*), and Teff (*Gzmb, Klrg1*) genes among clonally-related cells split by host. (f) Pre-rechallenge bulk TCR-seq of subset sorted T cells. Heatmaps are split by clone behavior determined by k-means clustering.
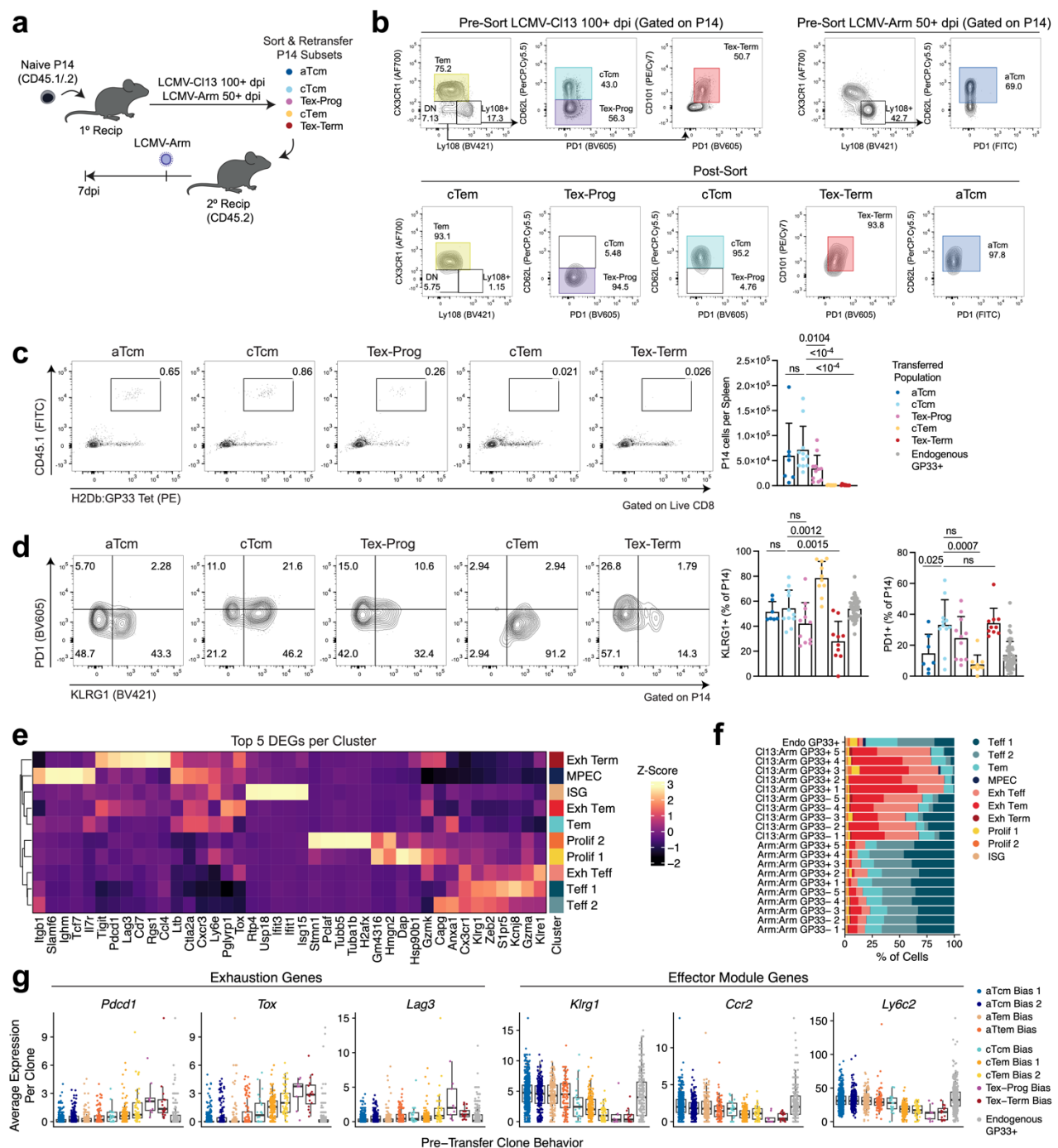
Extended Data Figure 7: Functional recall response of chronic Tcm.

(a-d) CD45.1$^+$CD45.2$^+$ P14 subsets were isolated from LCMV-Arm or LCMV-Cl13 immune chimeras and 2x10^3 cells were transferred into congenic hosts and challenged with LCMV-Arm. (b) Sorting scheme for P14 subsets and post-sort purity. (c) Flow cytometry quantifying recovery of P14s in secondary hosts 7dpi. (d) PD-1 and KLRG1 expression among P14 cells 7dpi. (a-d) Data are pooled from two independent experiments. Error bars show SD. n=7 aTcm, n=11 cTcm & Tex-Prog, n=10 cTem & Tex-Term. *P* values calculated by Mann-Whitney U Test. Data shown as mean+/-SD. ns=*P*>0.05. (e-g) scRNA/TCR-seq at 8 dpi from polyclonal Arm:Arm and Cl13:Arm rechallenge. (e) Top five differentially expressed genes (DEGs) per cluster in scRNA-seq of cells 8 dpi. (f) Cell frequencies from individual mice in cell clusters from scRNA-seq. (g) Expression of indicated genes from Cl13:Arm and Arm:Arm clones grouped by pre-transfer clone behaviors. Boxplots show Median, IQR, and 1.5xIQR.
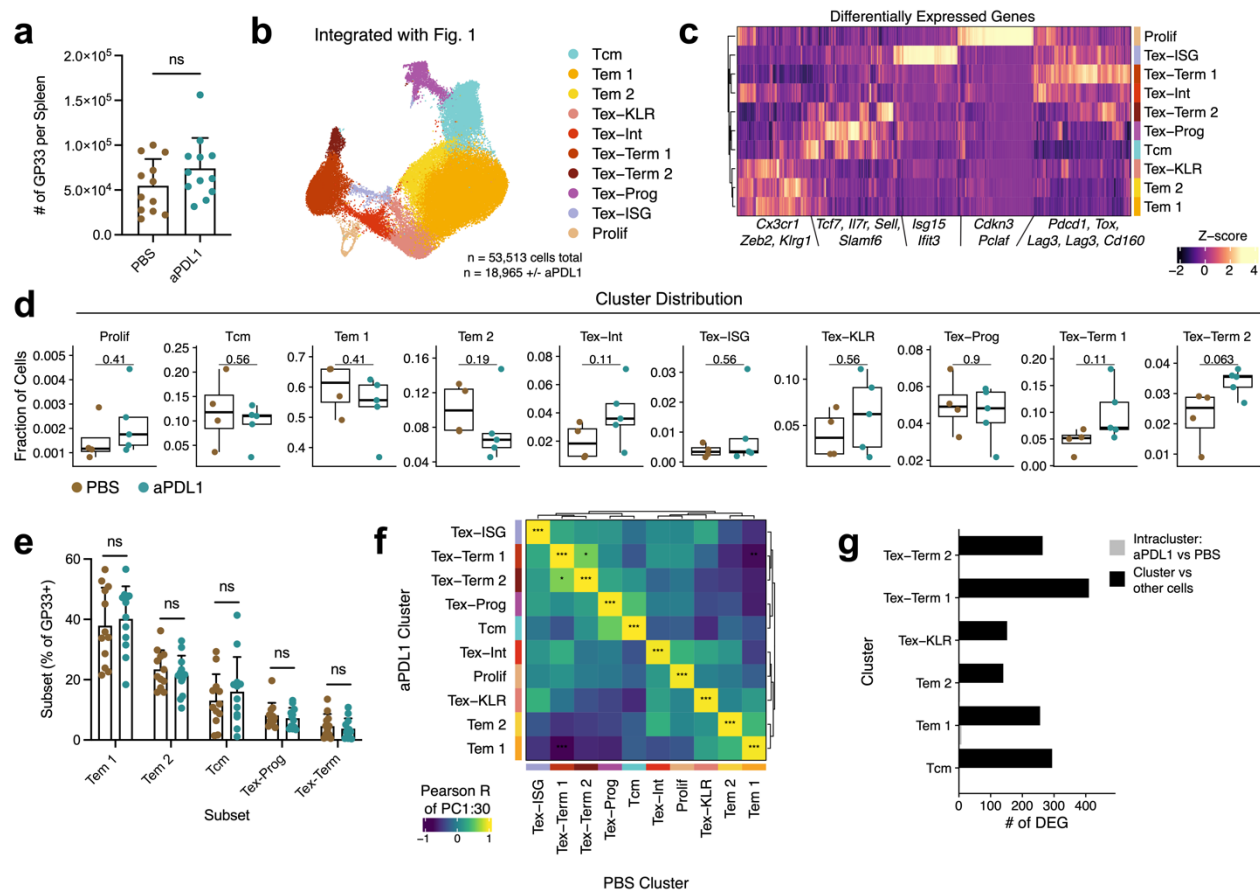
Extended Data Figure 8: αPD-L1 treatment does not impact cell states of chronic memory cells.
(a-g) Mice were infected with LCMV-Cl13 and treated with αPD-L1 from 22 to 34 dpi. Flow cytometry and scRNA/TCR-seq of GP33+ cells were performed at 100+ dpi. (a) GP33+ cell number at per spleen 100+ dpi. (b) UMAP of scRNA-seq profiles GP33+ cells from PBS and αPD-L1 treated mice integrated with data from **Fig. 1** colored by cluster. (c) Differentially expressed genes (DEGs) from cell clusters. (d) Cluster proportion from individual mice in each group. Boxplots show Median, IQR, and 1.5xIQR. (e) Cell subset frequencies of GP33+ cells by flow cytometry. (f) Pearson correlation of PCs 1-30 of cells in each cluster between groups (Bonferonni corrected *P* values). (g) Number of DEGs between cells within the same cluster from PBS vs αPD-L1 groups or between cells in cluster and all other cells. (a,e) n=12 mice/group. Data are pooled from two experiments. Bars show mean +/-SD. (b,c,d,f,g) n=4 mice PBS, n=5 mice αPD-L1. (a-g) Unless otherwise noted, *P* values calculated by Mann-Whitney U Test. *=*P*<0.05, **=*P*<0.01, ***=*P*<0.001,ns=*P*>0.05.

Methods

Animal studies

All mouse studies were carried out in specific pathogen free facilities at Stanford School of Medicine in accordance with protocols approved by the Stanford Institutional Animal Care and Use Committee (protocol number: 33814). All mice used were female mice on the C57BL/6J background. Wild-type (JAX000064) and CD45.1+ (JAX002014) and TCRα-/- (JAX002116) were purchased from Jackson Laboratories (Bar Harbor, ME). P14 TCR-transgenic mice were a gift from the Egawa Lab (Washington University, St. Louis) and crossed with C57BL/6J or CD45.1+ JAXBoy (JAX033076) mice for use in studies.

666

LCMV infections

Mice were generally infected at 7-12 weeks of age. Mice were infected with LCMV-Cl13 by intravenous retro-orbital (r.o.) injection with $2x10^6$ plaque forming units (pfu) or LCMV-Arm by intraperitoneal (i.p.) injection with $2x10^5$ pfu. The same dose of LCMV-Arm was used for infection of TCRα$^{-/-}$ mice. After 100 dpi LCMV-Cl13 infected mice were considered to have peripheral clearance of virus, however on occasion, viral titer remained high at this timepoint (**Extended Data Fig. 1a**), which was concordant with high (>75) % PD-1$^+$ among GP33$^+$ cells; these mice were excluded from experiments.

LCMV viral burden was quantified by qPCR as previously described[60]. Briefly, 250-500ng RNA extracted from Trizol (Invitrogen 15596-018) or spin columns (Zymo R1055) was used for cDNA synthesis (Quanta Bio 95048-100). qPCR was then performed with SYBR (BioRad 172-5275) and primers against LCMV-GP (fwd: cattcacctggactttgtcagactc, rev: gcaactgctgtgttcccgaaac) and quantified with a standard curve of linearized LCMV-GP containing plasmid (a gift from Miguel Sena-Esteves; Addgene 15793; ref[61]). To control for variability between experiments, LCMV viral burden data in **Fig. 4l** are presented as relative change from no transfer control.

αPD-L1 treatment

Treatments were performed by i.p. injection of 200ug αPD-L1 monoclonal antibody (BioXCell clone B7-H1) every 2-3 days from 22-34 dpi. Control mice were i.p. injected with PBS on the same schedule.

Cell isolation, flow cytometry, and cell sorting

Spleens were dissociated by mashing through 70-100µm filters into FACS buffer (PBS + 2% FBS + 1mM EDTA). Peripheral blood was collected r.o. with heparinized capillary tubes on anesthetized mice and blood was resuspended in FACS buffer. Cells were then either treated with ammonium chloride-potassium bicarbonate for red blood cell lysis or CD8$^+$ T cells were enriched by magnetic selection (StemCell 19853). Single cell suspensions were stained with GP33:H2D^b Tetramer (MBL) for 30 minutes in FACS buffer at room temperature followed by Live/Dead dye and surface antibody staining in FACS buffer for 20-30 minutes on ice. FC receptor blocking was performed prior to antibody staining either in Tetramer staining mix or during CD8$^+$ enrichment. For transcription factor staining, cells were fixed for 20 minutes in fixation / permeabilization buffer and stained for 1-2 hours in permeabilization buffer (eBioscience 00-5523-00). Prior to acquisition, stained cells were resuspended in FACS buffer and acquired on BD instruments (FACSAria III, Symphony, LSR-II). Sorting was performed with a BD FACSAria III into RPMI + 10-50% FBS at 4ºC. Purity was routinely confirmed ≥90%. Flow cytometry analysis was performed in FlowJo (BD), and counting beads (Invitrogen C36995) were used to quantify absolute cell numbers. Antibodies and other reagents for flow cytometry used are listed in **Supplementary Table 8**.

Adoptive T cell transfer

For all studies involving P14, naive CD8$^+$ T cells were isolated from spleen and lymph nodes of P14 TCR-transgenic mice by magnetic selection as described above with the addition of 3ug/mL biotinylated αCD44 (Biolegend, clone IM7). $2x10^3$-$4x10^3$ naive P14s were transferred per mouse. For other studies, CD8$^+$ enriched spleens or sorted T cell subsets were used. For all experiments, cells were resuspended in PBS and injected into recipient mice by r.o. Injection. In experiments with subsequent infection, mice were infected the following day with LCMV. For fate mapping into LCMV-free mice, P14 cells were first enriched by magnetic selection of APC-CD45.1$^+$ labeled cells (Miltenyi Biotec 130-090-855), followed by

712 sorting, and transfer into LCMV-immune mice infected with LCMV-Arm >3 weeks prior were used to
713 prevent carryover of virus[27,28].
714

Ex vivo quantification of cytokine secretion

716 $1x10^3$ sorted cells from GP33$^+$ subsets of T cells were resuspended in RPMI + 10% FBS. 50ng/mL
717 PMA and 1ug/mL ionomycin (Biolegend 423302) was added to wells to a final volume of 80uL. Cells were
718 stimulated at 37ºC for 18 hours. 3-5 replicates were plated for each sorted population. Supernatant
719 cytokine concentrations were assayed by cytokine bead array in duplicate (Biolegend 741050). Cytokine
720 concentrations were fit to the standard curve in Qognit LEGENDplex software and differential cytokine
721 production was calculated by `DESeq2` with cTcm as a control group.
722

scRNA/TCR-seq library preparation, data processing, and analysis

724 Prior to tetramer and antibody staining, CD8$^+$ enriched spleens were stained with MULTI-seq lipid
725 modified oligos (gift from Gartner Lab, UCSF) and barcodes as previously described[62], except with a
726 higher concentration of all reagents (μM) to accommodate increased cell number. Sorted CD8$^+$ T cells
727 were then pooled and up to 42,000 cells per well were loaded into a Chromium Controller and
728 encapsulated in GEMs with 5' v2 chemistry (10X Genomics 1000263). To improve integration, we
729 included landmark cells in each well (Naive for Fig. 1 and endogenous GP33$^+$ cells for Fig. 4) with a
730 unique MULTI-seq barcode. 5' scRNA, scTCR, and MULTI-seq libraries were prepared per
731 manufacturer's instructions or as previously described[62]. Indexed libraries were quantified using a Qubit
732 and Agilent Bioanalyzer and pooled per manufacturer's instructions. Pooled libraries were sequenced on
733 a NovaSeqX (Illumina) instrument with the following parameters: 28bp Read 1, 10bp Index 1, 10bp Index
734 2, 90bp Read2.
735 scRNA-seq data was processed using CellRanger Count (v3.1.0; 10X genomics) aligned to the mm10
736 genome. scTCR-seq data was processed with CellRanger VDJ (v6.0.0; 10X genomics) and the
737 `cellranger-vdj-GRCm38-alts-ensembl-3.1.0` reference. Additional processing and analysis was
738 performed with `Seurat` (v4.3.0). We filtered cells by `nFeature_RNA` (within 2 SD of mean and >1000),
739 `percent.mt` (< 95th percentile of dataset and < 4%), and biologically impossible TCR chain usage. After
740 filtering, we utilized `deMULTIplex2` to demultiplex samples and filter out doublets. We then performed
741 `NormalizeData` and `FindVariableFeatures` (n=2000) on each 10X sample. To integrate data from
742 multiple 10X samples, we implemented the reciprocal PCA pipeline. Integration features were found with
743 `SelectIntegrationFeatures`, and TCR, cell cycle, mitochondrial, histone, and ribosomal genes were
744 removed for all downstream analysis. Data was scaled and PCA was performed according to the
745 integration features, and we ran `FindIntegrationAnchors` and `IntegrateData` to generate a single object.
746 Seurat objects were then clustered and dimensionality reduction was performed by the standard pipeline.
747 Briefly, we ran `ScaleData`, `Run PCA`, `FindNeighbors`, and `FindClusters`. For all datasets, we found
748 clusters of low quality cells identified by high `percent.mt` and high or low `nFeature_RNA` or Naive cells
749 based on gene expression (high Tcf7 and Sell; low Cd44 and Cxcr3) and/or clustered with intentionally
750 sorted Naive cells. We removed unwanted cells and iteratively repeated clustering and dimensionality
751 reduction. Final clustering and dimensionality reduction parameters: Fig. 1, PC1:12, Resolution=0.4; Fig.
752 4, PC 1:10, Resolution=0.4; Fig. 5, PC1:15, Resolution=0.34.
753 To identify differentially expressed genes between clusters, we utilized `FindAllMarkers` (Wilcox Test,
754 LogFC cutoff=0.25) on variable features with TCR, cell cycle, mitochondrial, histone, and ribosomal
755 genes removed. To evaluate expression of exhaustion-related genes, we used `AddModuleScore` to
756 create a gene module of the common exhaustion module from ref[11] (**Supplementary Table 7**). To
757 evaluate pairwise correlations of gene expression within groups and clusters, we selected cells from the
758 most functionally important subsets of cells from each group, and found the median of each PC 1-30.

29

759 Pearson correlation was calculated on this matrix to find correlations between groups, and we applied
760 Bonferonni correction to *P* values. To find DEGs between aTem or cTem and other cells we grouped
761 cells by cell type (ie Tcm, Tem, Tex-Term, Tex-Int, Tex-Prog, Tex-KLR) and group. We used
762 `FindMarkers` (Wilcox Test, Log$_2$FC cutoff=0.25, *P*<0.01) on variable features with TCR, cell cycle,
763 mitochondrial, histone, and ribosomal genes removed.

764

765 ***Bulk TCR-seq library preparation and data processing***
766 TCR-seq was performed by Adaptive Biotechnologies and iRepertoire. For genomic DNA based
767 TCR-seq, samples were sorted, media was removed and cells were snap frozen. Immunosequencing
768 TCR-seq was performed by Adaptive at the survey depth. For RNA based TCR-seq, cells were sorted
769 into RNA lysis buffer (Zymo R1060) or DNA/RNA shield (Zymo R1100) and snap frozen. TCR-seq was
770 performed by iRepertoire via their RepSeq+ Platform. Different sequencing methods were selected on a
771 per-experiment basis based on trade-off of precision of absolute counts (better in genomic DNA-based),
772 and detection of rare clones (better in RNA-based).
773 For both TCR-seq platforms, TCR sequence by count files were imported into R (v4.3.1) for analysis.
774 For RNA-based TCR-seq, replicate libraries were amplified using each sample, so only TCR sequences
775 detected between replicates were analyzed. For each TCR, we used the total number of cells in a subset
776 and the clone's frequency in each subset to calculate the total clone size and each clone's phenotype
777 distribution.

778

779 ***ATAC-seq library prep, data-processing, and analysis***
780 For ATAC-seq, GP33+ T cells were subset sorted from mice at different timepoints. Pre-sort, cells
781 were combined into biologically distinct pools from multiple mice, and ATAC-seq was performed on these
782 biological replicates. Tex-Term cells were also sorted from mice with cleared LCMV-Cl13, however, cell
783 numbers were too low for reliable analysis.
784 Nuclei were isolated from 2,000-20,000 sorted T cells by resuspension in 50μL of Lysis Buffer (10
785 mM Tris-HCl pH 7.4, 10 mM NaCL, 3 mM MgCl$_2$, 0.1% Tween-20, 0.1% IGEPAL, 0.01% Digitonin, 1%
786 BSA) and spinning at 4ºC 600rcf for 10 minutes. Nuclei were resuspended in 25uL Transposase master
787 mix (2μL enzyme + 12.5μL 2X TD buffer + 10.5μL H$_2$O; Illumina 20034198) and incubated at 37ºC for 30
788 minutes with agitation at 400rpm. Tagmented DNA was isolated using MinElute PCR Purification Kit
789 (Qiagen 28004) and amplified with Illumina adapters (ApexBio K1058) using Phusion PCR master Mix
790 (New England Biolabs M0531S). Indexed libraries were size selected using SPRI (Beckman Coulter
791 B23318) and quantified by Agilent Bioanalyzer, and pooled at equimolar ratios. Libraries were sequenced
792 on a NovaSeqX (Illumina) instrument with 150bp paired end reads (1x10^8 per library).
793 ATAC-seq libraries were analyzed using `PEPATAC`[63] with default settings. Briefly, adapter
794 sequences were trimmed with `--trimmer {skewer}` followed by elimination of mitochondrial reads and
795 reads associated with repetitive genomic regions. The remaining reads were aligned to the mm10
796 reference genome using Bowtie2. SAMtools was used to extract uniquely mapped reads and duplicate
797 reads were removed using Picard; the resulting BAM files were used for downstream processing. OCR
798 calling for individual samples was performed with MACS2, and non-overlapping 500-bp OCRs (also
799 known as peaks) were generated. The OCRs by sample count matrix was constructed using default
800 settings of the `run_atac` function (ChrAccR). The matrix was variance-stabilized using the `vst` function
801 (DESeq2). Using the top 10,000 most variable OCRs, PC analysis plots were generated with `plotPCA`
802 (DESeq2) and samples were clustered by k-means clustering. Heatmap visualization was performed on
803 the same set of 10,000 OCRs and the OCRs were clustered based on k-means clustering. To assess
804 the number of differentially accessible OCRs between cTcm or Tex-Term and other cells, DESeq2 was
805 used with a Log$_2$FC cutoff of 1 and FDR cutoff of 0.01. For OCRs annotation to the nearest gene, the

806 function `annotatePeak` (ChIPseeker) was used. To find overlapping OCRs with data from ref[28], we
807 generated `GRanges` objects from .bed files of DARs in each cluster from their figure 5c provided by
808 authors, and found overlapping OCRs with our dataset using `findOverlaps` (GRanges). Genome
809 browser tracks were generated by aggregating data from replicate samples with `WiggleTools` and
810 plotting using `trackplot` and `ggplot2`.
811

Clone behavior analysis

813 To determine clone behavior of single GP33+ clones in scRNA/TCR-seq data, clones with a single
814 *Tcra* and single *Tcrb* chain with >1 (**Fig. 2a, Extended Data Fig. 3a, Extended Data Fig. 4a,b**) or >2
815 (**Fig. 5d**) cells were isolated. For determination of clone behaviors in GP33+ bulk TCR-seq data (**Fig 2b**),
816 we filtered expanded GP33+ clones with >4 cells sorted. For both data modalities, we clustered clones
817 with k-means clustering based on frequency of the clone in each phenotype to determine clonal
818 behaviors.
819 To determine if clones were significantly skewed towards any given phenotype versus the total
820 population of observed cells (**Fig. 2d**) we performed a hypergeometric test as established in ref[64].
821 Specifically, we calculated a one-sided hypergeometric test of each clone's frequency of the clone's most
822 frequent phenotype (n) compared to the total number of cells in the subset (N). We adjusted P values via
823 Hochberg correction.
824

Clone tracing between Tex and memory subsets

826 To determine if cTcm and other clone behaviors originated from clones present during chronic
827 infection, we compared repertoires of GP33+ clones at 100+ dpi to GP33+ sorted (89.3 % PD-1+;
828 **Extended Data Fig. 3d**) blood T cells at 28 dpi. To determine if clones from different behaviors are
829 differentially detected at 28 dpi, we performed a binomial logistic regression with `glm` and predicted if a
830 clone could be detected in blood (n≥1 cell) based on the independent variable of 100+ dpi clone behavior.
831 To assess the clonal origins of cTcm and other clone behaviors in the exhausted pool (**Fig. 2f-i**), we
832 analyzed subset sorted T cells from 21 and 100+ dpi. To expand breadth of response, we analyzed PD-
833 1+ clones at 21 dpi and considered all clones detected in 21 dpi PD-1+ subsets as LCMV-specific. We
834 restricted analysis to only clones >5 calculated sorted cells at both 21 dpi and 100+ dpi. To assess
835 similarities between subsets, performed Pearson correlation on a matrix of individual clones by subset
836 frequencies, adjusted P values with Bonferroni correction, and plotted correlations between subsets at
837 different timepoints. To determine how clone behaviors at 21 dpi gave rise to different subsets at 100+
838 dpi, we clustered the shared clones separately based on clonal subset distribution at each timepoint. For
839 the 100+ dpi timepoint, to resolve Tex-Prog and Tex-Term biased clones, we over-clustered (k=7) and
840 combined two cTem 1 biased clusters into the same behaviors. To determine which clones preferentially
841 formed cTcm biased clones, we performed logistic regression as described above with cTcm bias as the
842 dependent variable and 21 dpi clone behavior as the independent variable.
843 To evaluate if blood sampling gave a representative view of clonal behavior in the spleen, we sampled
844 PD-1+ Tex subsets from peripheral blood (collected via terminal cardiac puncture) and spleen of the same
845 mouse (**Extended Data Fig. d-h**). We analyzed clone size of all clones and filtered on clones > 10 sorted
846 cells in both organs to assess phenotype distribution between organs.
847

Clonal tracing during polyclonal CD8+ rechallenge

849 To determine the clonal response of Arm:Arm and Cl13:Arm cells, we enriched polyclonal CD8+ T
850 cells from three donor mice per group. Approximately half of cells were split into five recipient mice (2×10^5
851 cells per mouse) and rechallenged, and the remaining cells were subset sorted for TCR-seq.

852   The first aim of this experiment was to confirm that rechallenge responses were clonally biased as
853   has been shown in human memory T cells[41,43]. We isolated clones with a single *Tcra* and single *Tcrb*
854   sequence and performed Pearson correlation of relative clone size (frequency of total cells) for each
855   clone. To determine statistical significance, real clones were compared to a shuffled dataset where clone
856   size in each host was shuffled and compared all correlations by Mann-Whitney. To compare gene
857   expression profiles of clonally related cells in different hosts, we implemented PC correlation, which has
858   been used to assess clonal similarity of gene expression in clonally barcoded hematopoietic stem cells[65].
859   First, we isolated single *Tcra* and single *Tcrb* clones with >10 cells and calculated cell-cell correlation
860   based on the cell by PC correlation matrix for the PCs 1-30 of gene expression data. We then compared
861   correlation between clonal sisters in the same hosts and other hosts. To determine significance of this
862   correlation, we generated random clones by shuffling the clone id and compared this value to real clones.

863   To assess expansion of individual clones, we filtered clones single *Tcra* and single *Tcrb* clones which
864   were detected at both timepoints. We performed no further filtering for clonesize to ensure representation
865   of small clones. To assess expansion, we calculated the Log_2FC of post total number of cells per clone
866   at 8 dpi (clone frequency*total number of cells recovered) versus pre-rechallenge (clone frequency*total
867   number of cells transferred). To determine which clonal behaviors of cells expanded best upon
868   rechallenge, we performed k-means clustering of phenotype proportion data of Arm:Arm and Cl13:Arm
869   clones pre-rechallenge. Expansion of clones in different pre-rechallenge clone behaviors were compared
870   by Mann-Whitney U test.

871   To determine the gene expression profiles of cells from different pre-rechallenge clone behaviors, we
872   analyzed the same set of clones, and further filtered on clones with >4 cells in the 8 dpi dataset. We
873   calculated the probability of clones in a given pre-rechallenge behavior to derive clones predominantly in
874   the exhaustion-associated clusters (>50% of clone's 8 dpi progeny in `Exh Teff`, `Exh Tem`, or `Exh
875   Term` clusters) by logistic regression as described above (independent variable = pre-rechallenge clone
876   behavior, dependent variable = >50% in exhaustion-associated clusters). To determine how levels of
877   effector molecules differed among individual Cl13:Arm clones, we added an effector module based on
878   the top DEGs from the effector cell cluster (top 50 DEGs, filtered for presence in variable features in our
879   dataset) from $CD8^+$ T cells responding to LCMV-Arm infection (ref[11]; **Supplementary Table 7**) using
880   `AddModuleScore` (Seurat). To determine if individual clones had a significantly different effector module
881   score from the total distribution of Cl13:Arm cells, we performed a two-sided Mann-Whitney test with
882   Benjamini & Hochberg correction of individual clones versus the total distribution of Cl13:Arm clones as
883   established in ref[41]. We then quantified the number of clones with significantly ($P<0.05$) higher or lower
884   effector module score than the total distribution of Cl13:Arm cells.

885

Analysis of clonal behavior with αPD-L1 treatment

887   For clustering of clones in scRNA/TCR-seq after ICB (**Fig. 5d**), we over-clustered clones (k=8) and
888   combined multiple cTem 1 biased behaviors to resolve Tex-Prog and Tex-Term biased clones. To assess
889   clonal responses to αPD-L1 treatment, we analyzed subset sorted T cells from 21 dpi, 35 dpi, and 100+
890   dpi (**Fig. 5e-j**). Like with above, we assessed total T cells as to not restrict analysis to a single antigen
891   specificity, and analyzed only cells that were detected in $PD-1^+$ subsets at either 21 or 35 dpi. For all
892   analysis, we filtered clones on clones ≥10 sorted cells. We first assessed clonal behaviors of exhaustion
893   derived clones which we traced to the late timepoint. To determine longitudinal trajectories of clones, we
894   based analysis on the pipeline outlined in ref[48], which is designed to identify common behaviors of clones
895   at multiple timepoints. We modified this pipeline to take into account both total clone size and phenotype
896   proportion. We created a matrix of clones by phenotype frequency (clonotype subset count/total cell count
897   at timepoint) at all timepoints. To identify clones with common clonal trajectories over time, we calculated
898   Pearson correlation of each set of clones and performed hierarchical clustering of clones based on

32

899 euclidean distance of the correlation matrix. To link longitudinal trajectories to memory cell state, we
900 utilized a hypergeometric test to determine if clones were biased towards a phenotypic subset. We
901 calculated a one-sided hypergeometric test of each clone's frequency in each subset (n) compared to
902 the total number of cells in the subset (N). We adjusted P values via Hochberg correction, and clonal bias
903 was determined by a clones' lowest significant P value ($P<0.05$). To identify clone trajectory enrichment
904 the αPD-L1 group, logistic regression was performed as described above with group as the dependent
905 variable and clone behavior as the independent variable.
906

907 ***Statistical analysis***
908 All statistical analyses were performed in R (v4.3.1) and GraphPad Prism (v10). Statistical tests for
909 each experiment are noted in the above methods and/or figure legends. Unless noted, all statistical tests
910 were two-sided. No statistical testing was performed to pre-determine sample size.
911

912 **Supplementary Tables**
913 Supplementary Table 1 - Cluster DEGs of scRNA/TCR-seq from GP33^{+} atlas
914 Supplementary Table 2 - DEGs between cTcm or cTem and other subsets
915 Supplementary Table 3 - 10,000 most variable OCRs from ATAC-seq and Z-score accessibility per
916 sample
917 Supplementary Table 4 - DARs between Tex-Term or cTcm and other populations
918 Supplementary Table 5 - Cluster DEGs from scRNA/TCR-seq post rechallenge
919 Supplementary Table 6 - Cluster DEGs from scRNA/TCR-seq after aPDL1 treatment
920 Supplementary Table 7 - Gene module scores
921 Supplementary Table 8 - Flow cytometry reagents
922 Supplementary Table 9 - Source data
923

924 **Data Availability**
925 Raw sequencing data from this study are available on NCBI GEO at accession numbers GSE285411
926 (scRNA/TCR-seq atlas), GSE285412 (scRNA/TCR-seq αPD-L1), GSE285414 (scRNA/TCR-seq post-
927 rechallenge) and GSE285308 (ATAC-seq). Bulk TCR-seq data are available on Zenodo
928 (doi.org/10.5281/zenodo.14648171). Source data for other experiments are provided in **Supplementary**
929 **Table 9.**
930

931 **Code Availability**
932 No custom algorithms were developed for this study. Code and processed data needed to generate
933 figures from this study are publicly available online at GitHub at:
934 github.com/colinraposo/ChronicCentralMemory.
935

936 **References**
937 1. Wherry, E. J., Blattman, J. N., Murali-Krishna, K., van der Most, R. & Ahmed, R. Viral Persistence
938   Alters CD8 T-Cell Immunodominance and Tissue Distribution and Results in Distinct Stages of
939   Functional Impairment. *J. Virol.* **77**, 4911–4927 (2003).
940 2. Hashimoto, M. *et al.* CD8 T Cell Exhaustion in Chronic Infection and Cancer: Opportunities for
941   Interventions. *Annu. Rev. Med.* **69**, 301–318 (2018).
942 3. McLane, L. M., Abdel-Hakeem, M. S. & Wherry, E. J. CD8 T Cell Exhaustion During Chronic Viral
943   Infection and Cancer. *Annu. Rev. Immunol.* **37**, 457–495 (2019).
944 4. Wherry, E. J., Barber, D. L., Kaech, S. M., Blattman, J. N. & Ahmed, R. Antigen-independent
945   memory CD8 T cells do not develop during chronic viral infection. *Proc. Natl. Acad. Sci. U. S. A.*

101, 16004–16009 (2004).

5. Wherry, E. J. *et al.* Molecular Signature of CD8+ T Cell Exhaustion during Chronic Viral Infection. *Immunity* **27**, 670–684 (2007).

6. Gallimore, A. *et al.* Induction and Exhaustion of Lymphocytic Choriomeningitis Virus–specific Cytotoxic T Lymphocytes Visualized Using Soluble Tetrameric Major Histocompatibility Complex Class I–Peptide Complexes. *J. Exp. Med.* **187**, 1383–1393 (1998).

7. Zajac, A. J. *et al.* Viral Immune Evasion Due to Persistence of Activated T Cells Without Effector Function. *J. Exp. Med.* **188**, 2205–2213 (1998).

8. Jin, H.-T. *et al.* Cooperation of Tim-3 and PD-1 in CD8 T-cell exhaustion during chronic viral infection. *Proc. Natl. Acad. Sci.* **107**, 14733–14738 (2010).

9. Beltra, J.-C. *et al.* Developmental Relationships of Four Exhausted CD8+ T Cell Subsets Reveals Underlying Transcriptional and Epigenetic Landscape Control Mechanisms. *Immunity* **52**, 825-841.e8 (2020).

10. Hudson, W. H. *et al.* Proliferating Transitory T Cells with an Effector-like Transcriptional Signature Emerge from PD-1+ Stem-like CD8+ T Cells during Chronic Infection. *Immunity* **51**, 1043-1058.e4 (2019).

11. Daniel, B. *et al.* Divergent clonal differentiation trajectories of T cell exhaustion. *Nat. Immunol.* 1–14 (2022) doi:10.1038/s41590-022-01337-5.

12. Kasmani, M. Y. *et al.* Clonal lineage tracing reveals mechanisms skewing CD8+ T cell fate decisions in chronic infection. *J. Exp. Med.* **220**, e20220679 (2022).

13. Giles, J. R. *et al.* Shared and distinct biological circuits in effector, memory and exhausted CD8+ T cells revealed by temporal single-cell transcriptomics and epigenetics. *Nat. Immunol.* 1–14 (2022) doi:10.1038/s41590-022-01338-4.

14. Zander, R. *et al.* CD4+ T Cell Help Is Required for the Formation of a Cytolytic CD8+ T Cell Subset that Protects against Chronic Infection and Cancer. *Immunity* **51**, 1028-1042.e4 (2019).

15. Im, S. J. *et al.* Defining CD8+ T cells that provide the proliferative burst after PD-1 therapy. *Nature* **537**, 417–421 (2016).

16. Tsui, C. *et al.* MYB orchestrates T cell exhaustion and response to checkpoint inhibition. *Nature* **609**, 354–360 (2022).

17. Sen, D. R. *et al.* The epigenetic landscape of T cell exhaustion. *Science* **354**, 1165–1169 (2016).

18. Scott-Browne, J. P. *et al.* Dynamic Changes in Chromatin Accessibility Occur in CD8+ T Cells Responding to Viral Infection. *Immunity* **45**, 1327–1340 (2016).

19. Akondy, R. S. *et al.* Origin and differentiation of human memory CD8 T cells after vaccination. *Nature* **552**, 362–367 (2017).

20. Lau, L. L., Jamieson, B. D., Somasundaram, T. & Ahmed, R. Cytotoxic T-cell memory without antigen. *Nature* **369**, 648–652 (1994).

21. Zimmermann, C., Prévost-Blondel, A., Blaser, C. & Pircher, H. Kinetics of the response of naive and memory CD8 T cells to antigen: similarities and differences. *Eur. J. Immunol.* **29**, 284–290 (1999).

22. Veiga-Fernandes, H., Walter, U., Bourgeois, C., McLean, A. & Rocha, B. Response of naïve and memory CD8+ T cells to antigen stimulation in vivo. *Nat. Immunol.* **1**, 47–53 (2000).

23. Hensel, N. *et al.* Memory-like HCV-specific CD8+ T cells retain a molecular scar after cure of chronic HCV infection. *Nat. Immunol.* **22**, 229–239 (2021).

24. Pai, J. A. *et al.* Lineage tracing reveals clonal progenitors and long-term persistence of tumor-specific T cells during immune checkpoint blockade. *Cancer Cell* **41**, 776-790.e7 (2023).

25. Yates, K. B. *et al.* Epigenetic scars of CD8+ T cell exhaustion persist after cure of chronic infection in humans. *Nat. Immunol.* **22**, 1020–1029 (2021).

26. Tonnerre, P. *et al.* Differentiation of exhausted CD8+ T cells after termination of chronic antigen stimulation stops short of achieving functional T cell memory. *Nat. Immunol.* **22**, 1030–1041 (2021).

27. Charmoy, M., Wyss, T., Delorenzi, M. & Held, W. PD-1+ Tcf1+ CD8+ T cells from established chronic infection can form memory while retaining a stable imprint of persistent antigen exposure. *Cell Rep.* **36**, 109672 (2021).

28. Abdel-Hakeem, M. S. *et al.* Epigenetic scarring of exhausted T cells hinders memory differentiation upon eliminating chronic antigenic stimulation. *Nat. Immunol.* **22**, 1008–1019 (2021).

29. Schnoegl, D., Hiesinger, A., Huntington, N. D. & Gotthardt, D. AP-1 transcription factors in cytotoxic lymphocyte development and antitumor immunity. *Curr. Opin. Immunol.* **85**, 102397 (2023).

30. Graef, P. *et al.* Serial Transfer of Single-Cell-Derived Immunocompetence Reveals Stemness of CD8+ Central Memory T Cells. *Immunity* **41**, 116–126 (2014).

31. Buchholz, V. R., Schumacher, T. N. M. & Busch, D. H. T Cell Fate at the Single-Cell Level. *Annu. Rev. Immunol.* **34**, 65–92 (2016).

32. Buchholz, V. R. *et al.* Disparate Individual Fates Compose Robust CD8+ T Cell Immunity. *Science* **340**, 630–635 (2013).

33. Gerlach, C. *et al.* Heterogeneous differentiation patterns of individual CD8+ T cells. *Science* **340**, 635–639 (2013).

34. Grassmann, S. *et al.* Early emergence of T central memory precursors programs clonal dominance during chronic viral infection. *Nat. Immunol.* **21**, 1563–1573 (2020).

35. Sabatino, J. J., Jr., Huang, J., Zhu, C. & Evavold, B. D. High prevalence of low affinity peptide–MHC II tetramer–negative effectors during polyclonal CD4+ T cell responses. *J. Exp. Med.* **208**, 81–90 (2011).

36. Im, S. J., Konieczny, B. T., Hudson, W. H., Masopust, D. & Ahmed, R. PD-1+ stemlike CD8 T cells are resident in lymphoid tissues during persistent LCMV infection. *Proc. Natl. Acad. Sci.* **117**, 4292–4299 (2020).

37. Buenrostro, J. D., Giresi, P. G., Zaba, L. C., Chang, H. Y. & Greenleaf, W. J. Transposition of native chromatin for fast and sensitive epigenomic profiling of open chromatin, DNA-binding proteins and nucleosome position. *Nat. Methods* **10**, 1213–1218 (2013).

38. Wang, Q. *et al.* Exploring Epigenomic Datasets by ChIPseeker. *Curr. Protoc.* **2**, e585 (2022).

39. Yu, G., Wang, L.-G. & He, Q.-Y. ChIPseeker: an R/Bioconductor package for ChIP peak annotation, comparison and visualization. *Bioinformatics* **31**, 2382–2383 (2015).

40. Pauken, K. E. *et al.* Epigenetic stability of exhausted T cells limits durability of reinvigoration by PD-1 blockade. *Science* **354**, 1160–1165 (2016).

41. Mold, J. E. *et al.* Divergent clonal differentiation trajectories establish CD8+ memory T cell heterogeneity during acute viral infections in humans. *Cell Rep.* **35**, 109174 (2021).

42. Plumlee, C. R., Sheridan, B. S., Cicek, B. B. & Lefrançois, L. Environmental Cues Dictate the Fate of Individual CD8+ T Cells Responding to Infection. *Immunity* **39**, 347–356 (2013).

43. Mold, J. E. *et al.* Clonally heritable gene expression imparts a layer of diversity within cell types. *Cell Syst.* (2024) doi:10.1016/j.cels.2024.01.004.

44. Barber, D. L. *et al.* Restoring function in exhausted CD8 T cells during chronic viral infection. *Nature* **439**, 682–687 (2006).

45. Liu, B. *et al.* Temporal single-cell tracing reveals clonal revival and expansion of precursor exhausted T cells during anti-PD-1 therapy in lung cancer. *Nat. Cancer* **3**, 108–121 (2022).

46. Yost, K. E. *et al.* Clonal replacement of tumor-specific T cells following PD-1 blockade. *Nat. Med.* **25**, 1251–1259 (2019).

47. Singhaviranon, S., Dempsey, J. P., Hagymasi, A. T., Mandoiu, I. I. & Srivastava, P. K. Low-avidity T cells drive endogenous tumor immunity in mice and humans. *Nat. Immunol.* 1–12 (2025)

1040   doi:10.1038/s41590-024-02044-z.

48. Wang, K. *et al.* Combination anti-PD-1 and anti-CTLA-4 therapy generates waves of clonal responses that include progenitor-exhausted CD8+ T cells. *Cancer Cell* **42**, 1582-1597.e10 (2024).

49. Prokhnevska, N. *et al.* CD8+ T cell activation in cancer comprises an initial activation phase in lymph nodes followed by effector differentiation within the tumor. *Immunity* **56**, 107-124.e5 (2023).

50. Snell, L. M. *et al.* CD8+ T Cell Priming in Established Chronic Viral Infection Preferentially Directs Differentiation of Memory-like Cells for Sustained Immunity. *Immunity* **49**, 678-694.e5 (2018).

51. Shakiba, M. *et al.* TCR signal strength defines distinct mechanisms of T cell dysfunction and cancer evasion. *J. Exp. Med.* **219**, e20201966 (2021).

52. Schober, K. *et al.* Reverse TCR repertoire evolution toward dominant low-affinity clones during chronic CMV infection. *Nat. Immunol.* **21**, 434–441 (2020).

53. Hor, J. L. *et al.* PD-1 controls differentiation, survival, and TCR affinity evolution of stem-like CD8+ T cells. 2024.08.02.606241 Preprint at https://doi.org/10.1101/2024.08.02.606241 (2024).

54. McManus, D. T. *et al.* An early precursor CD8 T cell that adapts to acute or chronic viral infection. *Nature* 1–3 (2025) doi:10.1038/s41586-024-08562-y.

55. Chu, T. *et al.* Precursors of exhausted T cells are preemptively formed in acute infection. *Nature* 1–3 (2025) doi:10.1038/s41586-024-08451-4.

56. Watson, R. A. *et al.* Immune checkpoint blockade sensitivity and progression-free survival associates with baseline CD8+ T cell clone size and cytotoxicity. *Sci. Immunol.* **6**, eabj8825 (2021).

57. Wolchok, J. D. *et al.* Final, 10-Year Outcomes with Nivolumab plus Ipilimumab in Advanced Melanoma. *N. Engl. J. Med.* **0**, (2024).

58. Tran, C. *et al.* 1474 Cancer vaccine plus PD-1 blockade promotes infiltration of melanoma metastases by vaccine-induced T lymphocytes. *J. Immunother. Cancer* **10**, (2022).

59. Ott, P. A. *et al.* An immunogenic personal neoantigen vaccine for patients with melanoma. *Nature* **547**, 217–221 (2017).

60. McCausland, M. M. & Crotty, S. Quantitative PCR (QPCR) technique for detecting lymphocytic choriomeningitis virus (LCMV) in vivo. *J. Virol. Methods* **147**, 167 (2008).

61. Sena-Esteves, M., Tebbets, J. C., Steffens, S., Crombleholme, T. & Flake, A. W. Optimized large-scale production of high titer lentivirus vector pseudotypes. *J. Virol. Methods* **122**, 131–139 (2004).

62. McGinnis, C. S. *et al.* MULTI-seq: sample multiplexing for single-cell RNA sequencing using lipid-tagged indices. *Nat. Methods* **16**, 619–626 (2019).

63. Smith, J. P. *et al.* PEPATAC: an optimized pipeline for ATAC-seq data analysis with serial alignments. *NAR Genomics Bioinforma.* **3**, lqab101 (2021).

64. Li, L. *et al.* A mouse model with high clonal barcode diversity for joint lineage, transcriptomic, and epigenomic profiling in single cells. *Cell* **186**, 5183-5199.e22 (2023).

65. Singh, I., Perez, D. F., Sánchez, P. & Rodriguez-Fraticelli, A. E. Pre-existing stem cell heterogeneity dictates clonal responses to acquisition of cancer driver mutations. 2024.05.14.594084 Preprint at https://doi.org/10.1101/2024.05.14.594084 (2024).

Acknowledgements

Author Contributions

C.J.R., K.J.H-G, and A.T.S. conceptualized the study. C.J.R., K.J.H-G, and A.T.S. wrote and edited the manuscript with input from all authors. C.J.R., P.K.Y., S.M., and K.J.H-G. performed experiments. C.J.R., A.Y.C., and K.J.H-G. performed data analysis. K.J.H-G. and A.T.S. guided experiments and data analysis.

Declaration of Interests

A.T.S. is a founder of Immunai, Cartography Biosciences, Santa Ana Bio, and Prox Biosciences, an advisor to 10x Genomics and Wing Venture Capital, and receives research funding from Astellas and Northpond Ventures. All other authors declare that they have no competing interests.